Published in final edited form as:

Cell Rep. 2023 April 25; 42(4): 112376. doi:10.1016/j.celrep.2023.112376.

Conformational changes in the negative arm of the circadian clock correlate with dynamic interactomes involved in post-transcriptional regulation

Jacqueline F. Pelham[1,4], **Alexander E. Mosier**[1,4], **Samuel C. Altshuler**[1], **Morgan L. Rhodes**[1], **Christopher L. Kirchhoff**[1], **William B. Fall**[1], **Catherine Mann**[1], **Lisa S. Baik**[2], **Joanna C. Chiu**[2], **Jennifer M. Hurley**[1,3,5,*]

[1]Department of Biological Sciences, Rensselaer Polytechnic Institute, Troy, NY 12180, USA

[2]Department of Entomology and Nematology, University of California, Davis, Davis, CA 95616, USA

[3]Center for Biotechnology and Interdisciplinary Sciences, Rensselaer Polytechnic Institute, Troy, NY 12180, USA

[4]These authors contributed equally

[5]Lead contact

SUMMARY

Biology is tuned to the Earth's diurnal cycle by the circadian clock, a transcriptional/translational negative feedback loop that regulates physiology via transcriptional activation and other post-transcriptional mechanisms. We hypothesize that circadian post-transcriptional regulation might stem from conformational shifts in the intrinsically disordered proteins that comprise the negative arm of the feedback loop to coordinate variation in negative-arm-centered macromolecular complexes. This work demonstrates temporal conformational fluidity in the negative arm that correlates with 24-h variation in physiologically diverse macromolecular complex components in eukaryotic clock proteins. Short linear motifs on the negative-arm proteins that correspond with the interactors localized to disordered regions and known temporal phosphorylation sites suggesting changes in these macromolecular complexes could be due to conformational changes imparted by the temporal phospho-state. Interactors that oscillate in the macromolecular complexes over circadian time correlate with post-transcriptionally regulated proteins, highlighting how time-of-day variation in the negative-arm protein complexes may tune cellular physiology.

*Correspondence: hurlej2@rpi.edu.

AUTHOR CONTRIBUTIONS

Conceptualization, J.F.P., A.E.M., J.C.C., and J.M.H.; methodology, J.F.P., A.E.M., J.C.C., and J.M.H.; investigation, J.F.P., A.E.M., and L.S.B.; formal analysis, J.F.P., A.E.M., C.L.K., S.C.A., M.L.R.., W.B.F., and C.M.; writing – original draft, J.F.P. and A.E.M.; writing – review & editing, J.F.P., A.E.M., J.C.C., and J.M.H.; visualization, J.F.P., A.E.M., M.L.R., C.L.K., S.C.A., and W.B.F.; funding acquisition, J.C.C. and J.M.H.

DECLARATION OF INTERESTS

The authors declare no competing interests.

SUPPLEMENTAL INFORMATION

Supplemental information can be found online at https://doi.org/10.1016/j.celrep.2023.112376.

Graphical Abstract

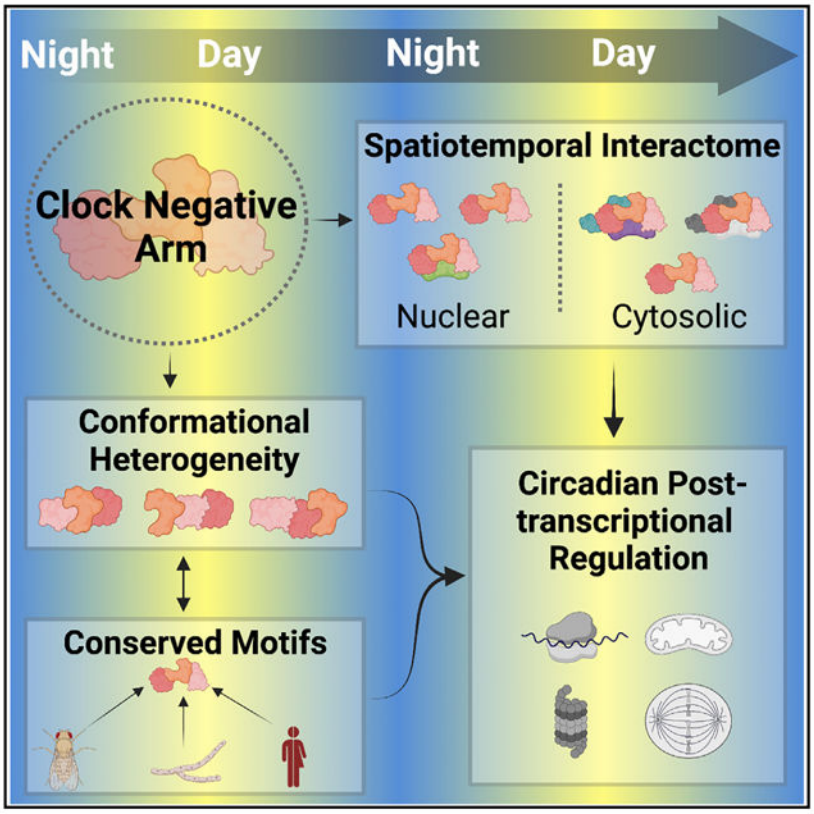

In brief

Pelham et al. show that negative-arm clock proteins are conformationally dynamic and impart spatiotemporal specificity. The predicted binding sites of negative-arm protein interactors correlate with protein disorder and post-transcriptional regulation, exemplifying a pathway of circadian physiological regulation stemming from negative-arm clock proteins.

INTRODUCTION

Most organisms subjected to the Earth's daily light/dark cycle have evolved a molecular mechanism to anticipate changes associated with this persistent oscillation in environmental conditions. This mechanism, called the circadian clock, increases survival, reproduction, and growth rates in organisms that maintain a clock.[1–3] At the molecular level, circadian clocks in both fungal and animal cells are regulated by a transcription/translation negative feedback loop (TTFL).[4,5] To complete a circadian cycle, the positive arm of the TTFL transcriptionally activates the negative arm, which in turn acts back on the positive arm to suppress this transcriptional activation, closing the loop. The negative arm is thought to set the length of the circadian cycle through a tightly regulated lifespan, controlling positive-arm reactivation.[4–8] To influence physiology, it has been postulated that the positive arm regulates gene promoters beyond the negative arm, controlling the rhythmic transcription of a large portion of the genome.[9–11] For this reason, research has predominantly focused on

time-specific transcriptional activation by the positive arm to identify circadian output.[4,12,13] However, recent research, including work in *N. crassa*, *D. melanogaster*, and humans, has demonstrated that many proteins show circadian oscillations, while their corresponding mRNA do not, though the source of this regulation is currently debated.[9,14–20]

Beyond negative-arm repression of the positive arm, the role of the negative arm in the regulation of output, if any, is not clear. What is known is that the negative arm forms a multitude of macromolecular complexes with a variety of proteins, including many that do not play a direct role in timekeeping.[21–24] This paradigm is true in the TTFL of fungal, insect, and mammalian cells, where the core negative-arm proteins, FREQUENCY in fungi (FRQ), and the PERIODs in animals (PERs) have been demonstrated to have a wide array of interactors, only some of which impact core clock functions.[21,23,25–28] The conservation of large interactomes in negative-arm clock proteins is not surprising, as negative-arm proteins from eukaryotic clocks are largely intrinsically disordered proteins (IDPs).[6,29–33] IDPs are a class of proteins known for their dynamic and heterogeneous ensemble of conformations whose inherent flexibility adds to their abilities to bind, facilitating more extensive and transient interactomes compared with globular proteins.[34–42] Due to promiscuity in binding and demonstrated disorder, we hypothesized that negative-arm proteins possess temporal-specific conformational ensembles that time protein-protein interactions, allowing the negative arm to act as a temporal “Hub” protein to impart post-transcriptional regulation of output.[43–45]

To investigate this hypothesis, we surveyed FRQ from *N. crassa* in its microenvironment over circadian time with the circadian native fast parallel proteolysis (CRAFTY) approach, using altered protease accessibility as a proxy to ascertain that the conformations of FRQ temporally oscillated.[30] We coupled this with an investigation of the protein complexes centered around FRQ over the circadian day, demonstrating that the interactors correlated with conformational changes in FRQ and localized to disordered regions in the protein. To extend this paradigm to the negative arm in higher eukaryotes, we surveyed the complexes centered around the functional analog of FRQ in *D. melanogaster* (dPER) and humans (hPER2),[21] demonstrating that complexes centered around dPER are spatiotemporally specific and correlate with disordered regions. Among these negative-arm interactors, there was an enrichment for proteins that had regions of intrinsic disorder, with temporal-specific disorder-to-disorder interactions occurring at the nadir of post-transcriptionally-regulated circadianly oscillating proteins, signifying that negative-arm proteins may play a role in proteostasis to synchronize the cell post-transcriptionally. Moreover, interactors played a variety of regulatory roles in the cell, suggesting potential pathways of post-transcriptional regulation beyond proteostasis.

RESULTS

CRAFTY analysis demonstrates oscillations in the FRQ conform-ome

IDPs are difficult to characterize using typical structural approaches due to conformational heterogeneity and instability during overexpression. Therefore, to demonstrate temporal changes in the ensemble of conformations (referred to here as the “conform-ome”) of the negative arm, we applied the CRAFTY approach to FRQ.[30] CRAFTY analyzes the

average changes in the conformations of a protein in a “native” lysate over circadian time to determine protein conformation, utilizing digestion/protease accessibility as a proxy for the protein microenvironment.[30,36] We performed CRAFTY on age-matched *N. crassa* mycelial mats from a strain where the C-terminal end of FRQ was fused to a V5–10His-3FLAG tag inserted at the cyclosporin locus of an FRQ knockout (KO) strain (τ = 21.3 ± 0.39 h) (strain WT8–1) (Figure S1A) (see STAR Methods). Mats were shifted to constant darkness (DD) before being sampled every 4 h for 24 h in triplicate over circadian time (Figure S1B). Whole-cell lysates were processed through CRAFTY in parallel, analyzed by western blot, and quantified to determine the degradation rate of FRQ (Figure S1C) (see STAR Methods). Our analysis found that the rate of FRQ digestion varied over circadian time, with the most protease resistance at CT13.6 (~155 s) and the least at CT9.3 and CT22.1 (~60 s) (Figures 1A, gray, and S1C). This shift from a closed to an open conformation correlated with the progressive phosphorylation of FRQ, though increasing phosphorylation did not necessarily represent increasing protein accessibility at all time points, as has been reported previously.[22,46]

Macromolecular complexes centered around FRQ vary in concordance with changes in the FRQ conform-ome

We hypothesized that the changes in the conform-ome of FRQ could be related to qualitative and quantitative changes in the proteins in FRQ macromolecular complexes. To validate this hypothesis, we utilized a strain with a V5–10His-3FLAG epitope-tagged FRQ allele inserted in the native FRQ locus (strain 1500–1) (τ = 24.9 ± 3.3 h) (Figures S2A, S2C, and S2D). Using both the 1500–1 strain and a wild-type strain as a control (Ku70a), *N. crassa* was sampled over circadian time, with samples taken from constant light (LL) and 4, 8, 12, 16, 20, and 24 h after the light to dark transition (DD) (Figure S2B). Macromolecular complexes centered on FRQ were purified from each time point via a two-step Ni^+ agarose/αFLAG co-immunoprecipitation process and validated to bind to known FRQ-interacting partners WC-1, WC-2, and FRH (Figures S2C and S2D). Co-immunoprecipitated proteins were analyzed using nanospray liquid chromatography-mass spectrometry/mass spectrometry (NS-LC-MS/MS) (see STAR Methods). The standard for detection from the NS-LC-MS/MS results was based on an empirical analysis of known FRQ-interacting proteins, and proteins were only included in the dataset if they had ≥5% total protein coverage or ≥4 unique peptides at a given time point in scaffold. We further refined this list by eliminating proteins that were detected in less than two of the three triplicates at a given time point in the 1500–1 strain or detected in any Ku-70 time points (Figure S2E; Table S1; Mendeley Data link in key resources table).

As expected, FRQ was identified in all samples from the 1500–1 strain (Figure S3A), and known FRQ-interacting partners FRH, CK-1, WC-1, and WC-2 were detected throughout the circadian day (Table S2). 681 FRQ protein-protein interactions were identified, 658 of which were novel FRQ protein-protein interactions (Table S1, compared with Baker et al.[22]). Only three proteins beyond the FRQ-FRH complex were found at all time points, and eight additional interactors were found across four or more time points (Figure S3A; Table S2). Conversely, 433 proteins were unique to a single circadian time point, with the number of interacting partners varying from as few as 22 interactors at CT5.07/DD16 to as many as

357 interactors at CT13.6/DD24 (Figures 1B and S8; Tables S1 and S2). When we compared the peak of protease resistance via our CRAFTY analysis with the peak of protein-protein interactions with FRQ via our NS-LC-MS/MS analysis, we found that peak interaction aligned with peak protease resistance (Figure 1A). We further assessed the 1500–1 strain using CRAFTY and showed that this oscillation was repeatable in this strain and over a longer time span (Figure S1D).

We next compared the FRQ-centered macromolecular complexes from LL with the FRQ-centered macromolecular complexes from DD (Table S1). We found that while 20 proteins were involved in FRQ macromolecular complexes in both LL and DD samples, 94 proteins were specific to LL FRQ macromolecular complexes, and 567 proteins were specific to DD FRQ macromolecular complexes (Figure 1C). These data support previously published work demonstrating a difference between LL and DD FRQ.[22,48,49]

Predicted short linear motifs in FRQ-centered macromolecular complexes cluster in disordered regions

IDPs are known to facilitate binding through conserved short linear motifs (SLiMs), regions less than 15 residues in length that are characterized by residue-pattern conservation in regions with otherwise low levels of explicit sequence conservation.[40,50,51] Post-translational modifications (PTMs) commonly regulate SLiMs,[52,53] and FRQ has over 100 identified phosphosites, mainly in the disordered regions of FRQ (Figures 2A and 2B).[22,30,31,52,53,54–56] To determine if there was a correlation between SLiMs, disorder, and phosphorylation in FRQ, we computationally investigated the characteristics of FRQ that emerge from its primary sequence to dictate its function, which we will refer to as molecular grammar, using a eukaryotic linear motif (ELM) predictor with a taxonomic context filter specific for the fungal kingdom and a motif probability cutoff of 100.[57] We then manually curated the ELM-predicted SLiMs by removing any for which a known SLiM binder was not identified in the FRQ interactome. The remaining SLiMs were mapped to a linear representation of FRQ in addition to the known phosphorylation sites from Baker et al.[22] (Figures 2B and 2E). Thirteen FRQ-interactor-specific SLiMs were identified, color coded by class, and mapped to their position (or positions if identified in multiple locations) on FRQ (Figures 2B and 2E). We then plotted the predicted regions of disorder and disordered-to-order transition in FRQ using IUPred2A(L) and ANCHOR2, respectively (Figure 2A). We found that SLiMs for validated FRQ interactors were ubiquitously found in regions of disorder, with a high tendency of disordered to ordered transition, and in regions that were near or at validated phosphorylation sites (Figure 2).

Macromolecular complexes in higher eukaryotes are spatiotemporally specific, regulated by phosphorylation, and centered in disordered regions

To determine if the correlation between SLiMs and regions of disorder was conserved in higher eukaryotes, we performed affinity purification coupled with MS/MS to survey the macromolecular complexes centered around *Drosophila* PERIOD (dPER) in a 12-h light and 12-h dark (12:12 LD) entrainment scheme. To do so, dPER was immunopurified at Zeitgeber time (ZT) 3, 16, 20, and 24 via a 3xFLAG antibody from cytosolic and nuclear fractions from *D. melanogaster* heads in an N-terminal, 3xFLAG-tagged dPER line with an

untagged line as a control. Samples were then analyzed by MS/MS and proteins with ≥4 unique peptides in at least 2 out of 3 replicates in the 3xFLAG-tagged dPER, but not the untagged line, were considered valid dPER interactions. As expected, we found TIMELESS (TIM) and DOUBLETIME (DBT) in all time points (Table S3; Mendeley Data link in key resources table). In addition to TIM and DBT, 248 unique proteins were detected in complex with dPER (Figures 3A and 3B; Table S3), but only three of these were found in complex with dPER at all time points, suggesting that like FRQ, dPER has an extensive and temporally regulated interactome. Of the 248 interactions, 89 and 115 proteins were unique to the nucleus and cytosol, respectively (Figure 3B; Table S3).

We next computationally investigated the molecular grammar of dPER for the tendency for disorder, disordered to order transition, and SLiMs using IUPred2A(L), ANCHOR2, and an ELM predictor as above, identifying 14 SLiMs (Figures 2C–2E). Moreover, we similarly surveyed the molecular grammar of hPER2 based on interactors from a previously published study, identifying 18 SLiMs (Figure S4).[21] In both cases, the majority of SLiMs mapped to regions with a higher tendency for protein disorder and phosphorylation, suggesting that the IDP nature of the negative-arm proteins in the clock is conserved because the characteristics of disordered proteins may allow for the regulated phosphorylation and SLiM binding that is essential for the clock to regulate cellular physiology (Figures 2 and S4).

To investigate the effect of phosphorylation of negative-arm proteins on their interactomes, we repeated our interactome analysis on a *Drosophila* strain with an internal deletion in the DBT binding domain on dPER (755–809) (dPER Δ) that results in strain arrhythmicity and altered phosphorylation (see STAR Methods).[59] 3xFLAG-tagged dPER and dPER Δ had 148 interactors in common and 103 and 61 interactors unique to dPER and dPER Δ, respectively (Figure 3C). There were further differences between dPER and dPER Δ when comparing spatiotemporal interactions, suggesting an important role for DBT and phosphorylation in both the location and timing of complex constituents (Figures 3D and 3E; Table S3; Mendeley Data link in key resources table).

Conserved interaction classes suggest diverse regulatory roles for negative-arm complexes

Given the time-of-day-specific macromolecular complexes that form in the negative arm, and given that disordered scaffold proteins have been suggested to serve as “Hub” proteins, highly connected proteins that are essential in a protein-protein interaction network, we proposed that the clock negative-arm proteins are biophysically suited to act as a temporal “Hub” protein.[60,61] To investigate the physiological effect the negative arm could impart post-transcriptionally by acting as a time-specific “Hub” protein, we surveyed the interactor/SLiM-class parings conserved across our datasets at the single SLiM level. One common SLiM class, the highly conserved 14-3-3 binding motif, which is recognized by 14-3-3 class proteins that identify and phosphorylate substrates in disordered regions to regulate cell division and other processes, was seen in flies, *Neurospora*, and humans (Figures 2B, 2D, 3, and S4B).[62–70] Correspondingly, 3 hPER2 and dPER 14-3-3 SLiMs resided in regions of disorder (Figure 2).[71] Of note, 14-3-3 proteins were not among the dPER Δ interactors,

emphasizing the importance of phosphorylation in regulating the formation of negative-arm "Hub" complexes.

Consistent with the importance of phosphorylation, 21, 12, and 16 kinases were found in complex with FRQ, dPER, and hPER2, respectively, and phosphorylation SLiMs aligned with many of the experimentally verified phosphorylation sites (Tables S1 and S3).[22,54,72] Since not all kinases found in negative-arm macromolecular complexes target the negative arm, these kinases may serve to phosphorylate other negative-arm binding proteins to affect cellular physiology.[22,54–56] For example, cyclin-dependent kinase cell division control protein 2 (CDC-28) in *N. crassa*, a homolog of human CDK-1, acts as a cell cycle gatekeeper and must be phosphorylated before the cell can transition beyond S- and M-phases.[73–75] CDC-28 (NCU09778) was identified as an FRQ interactor at CT20.53/DD8, the time known to correlate with the clock regulation of entry to S-phase and the same time as the zenith of several post-transcriptionally rhythmic S-phase-associated proteins (MCM3, MCM4, and ORC3) (Table S1; Figure S5).[76]

To explore the resonating effects of temporal changes to the macromolecular complexes centered around FRQ and dPER at the interactome level, we created a program that utilizes the STRING database to generate a temporal protein-protein interaction network (PIN) based on our interactome analysis.[77] Our PIN employed gene ontological (GO) analysis to assign interactor functions using the TopGo package adapted from our Multi-Omics Selection with Amplitude Independent Criteria (MOSAIC) program and PANTHER to assign GO terms to each primary interactor for both dPER and FRQ, with predicted secondary interactors for FRQ (Figures 4A, S5, and S6).[78–81] For ease of visualization, the program only reported GO terms if the GO term had at least 20 assigned proteins. The PIN maps displayed the different impacts in biological effect that negative-arm macromolecular complexes may have at different circadian time points and in different cellular compartments (Figures 4A, S6, and S7). We also created word clouds to represent the magnitude of enrichment of each of the interactor GO categories for FRQ, dPER, and hPER2 (Figures 4B–4D).

We found that metabolic GO terms accounted for the majority of interactors of FRQ between CT5.1 and CT13.6 but fell below 50% later in the circadian day (Figure 4A; Table S2). The timing of the increase in metabolic proteins in FRQ macromolecular complexes correlated with known post-transcriptional regulation of metabolism in the circadian evening in *N. crassa*.[19] Further, our analysis also showed enrichment for RNA binding and structural constituents of the ribosome in *N. crassa*, *D. melanogaster*, and humans, including the 60S ribosomal protein L8 and several eukaryotic initiation factors that are found in all three datasets (e.g., dPER: RpL8, FBgn0261602; hPER2: RPL8, P62917; and FRQ: *crp-41*, NCU4779) (Figures 4B–4D; Tables S1, S2, and S3). This is important, as a cause of circadian influence on post-transcriptional regulation has been traced to translational rates.[19,20,82]

IDP/IDP interactions may impart circadian post-transcriptional regulation

IDPs are known to be stabilized through interactions with their binding partners, and proteostasis is predicted to be circadianly regulated.[83–87] Therefore, beyond the role

of the negative arm as a “Hub” protein, another possible mechanism for circadian post-transcriptional regulation could be the regulation of the half-life of negative-arm interacting proteins. Though order- to disordered-region binding is more frequently described in the literature, recent data have shown that IDPs can interact with other IDPs to affect molecular change.[88] We hypothesized that negative-arm binding to IDPs could lead to post-transcriptional regulation of these IDPs via proteostasis, and, if so, IDPs would be overrepresented in the interactomes. To determine how pervasive these IDP/IDP interactions were, we examined the extent the proteins found in complex with the negative arm were disordered. Four disorder predictors (VLXT, VSL2b, IUPred2A(L), and PV2) were used to predict disorder in interactors, and the average disorder score was used to classify each interactor as either an IDP (disordered score > 30%), a protein with disordered regions (PDR; disordered score <30% with 30 residue disordered ends or 40 residue disordered internal regions), or an ordered protein (OP; disordered score <30% with no end or internal disordered regions), as was defined by Deiana et al. (Table S4).[58,89–95]

In the case of FRQ, just under half (267, or 45.5%) of interactors were defined as IDPs by our classification (Figure S3B). As we determined that the *Neurospora* proteome was comprised of 54.5% IDPs, IDPs were significantly underrepresented in FRQ macromolecular complexes, contrary to our prediction (Fisher’s exact test $p < 10^{-5}$) (Figure S3B). Conversely, PDRs and OPs were overrepresented in the FRQ interactome (Fisher’s exact test $p < 0.004$) (Figure S3B). We next examined the interactor disorder classification (IDP, PDR, and OP) by time of day of binding to FRQ. Contrary to the underrepresentation of IDPs in the overall dataset, IDPs were enriched in the late circadian night/early circadian morning, while IDPs/PDRs/OPs were more evenly distributed in the late circadian morning/early circadian afternoon, suggesting a circadian rhythm to the binding of IDPs (Figure 5A; Table S5). To determine if stoichiometric ratios could explain the time-of-day-specific increase in FRQ/IDP interactions or if these proteins may represent cases of circadian post-transcriptional regulation due to FRQ-induced stabilization, we identified interactors that were reported to oscillate with a circadian period at the protein level (Table S5).[19] When we empirically compared the interaction time with the zenith of the corresponding protein levels of FRQ interactors, we found through qualitative observation that PDRs and OPs interacted with FRQ at their zenith, while IDPs predominantly interacted with FRQ during their nadir (Figures 5B–5D). This suggests that FRQ/IDP interactions are timed to occur at the IDP nadir levels rather than occurring based on passive interaction due to stoichiometry.

Though we did not have temporal proteomic data to compare, we performed a similar analysis to quantify the extent of intrinsic disorder in dPER macromolecular complexes. Unlike FRQ, there was no enrichment or depletion of OPs, IDPs, and PDRs in the dPER interactome (Figure 5E; Table S5). However, the nuclear dPER fraction displays a circadian pattern of interaction with IDPs, with a significant enrichment of IDPs at ZT 20 and 24 (Figure 5F; Table S5).

DISCUSSION

A discrepancy between the circadian oscillations of mRNA and their cognate proteins has been established, though the mechanisms of this post-transcriptional regulation remain

elusive.[14–16,19,20] As we and others have shown that negative-arm proteins can modulate conformation over the circadian day, we hypothesized that the conserved intrinsic disorder documented among negative-arm proteins could allow for conformational changes that correlate with changes in negative-arm protein-protein interactions to effect circadian post-transcriptional regulation.[29–31,46,96] To validate this hypothesis, in this article, we performed a CRAFTY analysis of the FRQ conformation over circadian time, a temporal analysis of the macromolecular complexes centered around FRQ and dPER using MS/MS, and mined data from previous analyses on hPER2 interactors.[21] While the mechanistic relationship between shifts in the FRQ macromolecular complexes and the FRQ conform-ome remain unclear, the conformational variations of the negative-arm protein FRQ correlated with the peak numbers of interactors identified in our investigation (Figure 1). In concordance with this, the extent of proteins involved in negative-arm macromolecular complexes, the role of phosphorylation in dPER protein complexes, and the demonstration that SLiMs were in disordered and phosphorylated regions (Figures 1, 2, 3, and S4) suggest that changes in phosphorylation states of negative-arm proteins allow for variations in the availability of negative-arm SLiMs and thereby the components of macromolecular complexes. Changes in the availability of SLiMs could also influence the availability of phosphorylation sites, and so a mechanistic approach will be important in determining the direction of influence a flexible conformation has on the relationship between SLiMs and phosphorylation in clock proteins. Though our methods cannot determine if the identified interactions are direct, and it is important to note that the methods that we used could have detected some spurious binding with the epitope tags or through stochastic interactions, our computational analysis showed that many interactors had cognate SLiMs and that oscillating disordered proteins tended to interact with FRQ when they were at their lowest levels, providing some evidence that many of the proteins may directly interact with FRQ, dPER, and hPER in the native context. As many eukaryotic negative-arm clock proteins are known to be IDPs, we propose that disorder in the negative-arm proteins allows for conformational flexibility that times the formation of macromolecular protein complexes in all eukaryotic clocks to impart temporal information (Figure 6).[31] For example, the negative arm brings together kinases and their targets at specific points of the circadian day (Figure 6).

Many of the identified interactors regulate downstream pathways that are known to be under circadian post-transcriptional regulation and can themselves be regulated by phosphorylation.[19] For example,14-3-3 zeta, a regulator of the c-Raf pathway, has been shown to be phosphorylated by CK1.[97,98] Further, the phosphorylation of CDC-28 is known to be one of the synchronizing links between the circadian and cell cycles, and the timing of its interaction with FRQ could facilitate temporal specificity of this transition between cell cycle phases.[76] Therefore, our work suggests that the negative arm may act as a “Hub” protein to concentrate protein-protein interactions temporally to impart phosphorylation events on interactors in a circadian manner. This temporal “Hub” model, and the spatiotemporal specificity conferred by DBT (Figure 3), aligns with the suggested dPER foci heterogeneity speculated by Xiao et al.[99] This could explain how circadian proteins are detected from non-circadian transcripts, and vice versa. How the negative-arm FRQ-/dPER-centered complex could sequester or time phosphorylation of these IDPs is unclear. However, the formation of a “clocksome” through the timed creation

of biomolecular condensation centered on the negative arm and mediated by IDRs for circadian post-transcriptional regulation is a tempting model.[100,101]

Alternatively, or perhaps in parallel, our data also suggest a mechanism by which the negative arm temporally stabilizes interacting IDPs to impart post-transcriptional regulation. While our predictions of protein disorder among interactors showed that IDPs were underrepresented in our dataset, many proteins that were IDPs interacted with FRQ at the nadir of their expression, suggesting that the negative arm may stabilize the protein to impart post-transcriptional regulation (Figure 5). This correlated with recent data showing the importance of the clock in proteostasis.[86,87] Importantly, our two models of negative-arm post-transcriptional regulation, the “Hub” model and the “stabilization” model (Figure 6), are not mutually exclusive and do not necessitate a direct interaction between the negative arm and its cognate interactors, simply that a negative-arm-regulated interaction occurred in the correct time and space.

Regardless of the mechanism by which the negative arm imparts post-transcriptional regulation, FRQ, dPER, and hPER have extensive interactomes, with functions that range across diverse gene ontologies (Figure 4). This aligns with the large and variable interactomes that are a hallmark of negative-arm proteins throughout eukaryotic circadian clocks.[23,27,31,102–105] In FRQ, we found that 58 interactors, more than half of which (33) were IDPs, have rhythmic proteins without corresponding rhythmic mRNA. These 58 proteins accounted for ~11% of all post-transcriptional regulation (rhythmic protein/mRNA discrepancies) reported in Hurley et al.[19] Further, many other FRQ interactors are responsible for regulating proteins under circadian post-transcriptional control.[19] In total, this suggests that negative arm-based post-transcriptional regulation could have great physiological reach, and future research in the lab will focus on the validation and effect of this regulation.

Limitations of the study

In this study, we performed *ex vivo* proteolysis and co-immunoprecipitation. Due to the limitations of these approaches, we acknowledge that other confounding factors may influence protease accessibility and the transient interactions of our target proteins. For example, as proteins co-immunoprecipitated (coIPed) from protein lysates have an intrinsic bias for soluble proteins, negative arm-membrane protein interactions may have been lost in our analysis, and the negative-arm interactome may be larger than we report. Furthermore, the error inherent to informatic analysis may impact the validity of the predicted interactions, e.g., false discovery rate (FDR) rate cutoffs may either over- or underestimate the number of valid interactions.

STAR★METHODS

RESOURCE AVAILABILITY

Lead contact—Further information and requests for resources and reagents should be directed to and will be fulfilled by the lead contact, Jennifer Hurley (hurlej2@rpi.edu).

Materials availability—All of the unique strains generated in this study are available from the lead contact without restriction.

Data and code availability

- Additional mass spectrometry data and raw western blot data and images can be found on Mendeley data: https://data.mendeley.com/datasets/cshd5drzp5/draft?a=99cee2fb-f059-40f3-b825-ce9f3f0badff.
- Versioned code for generation of PPIN maps can be found on the Zenodo repository: https://doi.org/10.5281/zenodo.7741908
- Any additional information required to reanalyze the data reported in this work paper is available from the lead contact upon request.

EXPERIMENTAL MODEL AND SUBJECT DETAILS

***Neurospora crassa* strains, plasmids, and reagents—**Five strains of *N. crassa* were used in this report (STAR Methods). The cassette for strain WT8–1 was assembled as described in Colot et al. 2006, and transformed into an *frq* null (Δ*frq*, *bd*$^{+}$, mat a) background at the *cyclosporin resistant-1 (csr-1)* locus to create the genotype *csr-1::frq*^{v5his103flag}. To create this construct, starting at the 5′ end, we fused 1000 bps from the upstream portion of *csr-1*, (NCU00726), to 3000 bps upstream of the *frq* promoter spanning to the *frq* open reading frame, excluding the stop codon. This sequence was followed by an epitope fusion of a 10x glycine linker, a V5 sequence, 10xHis, and a 3xFlag sequence followed by a stop codon. Next, 1000 bps downstream of the *frq* ORF was fused to the stop codon, concluding with 1000 bps from the downstream portion of the target *csr-1* locus. Strain 1500–1 was created by transformative recombination at the native *frq* locus to fuse a V5–10His-3FLAG tag with an *hph* cassette to the C-terminal end of the protein FRQ (*frq*^{V5H103FLAG}*::hph+, mus52::bar*). Transformations were performed as described[115,116] and screened by PCR. The negative control strain for our mass spectrometric analysis was Ku70a. Race tube analysis of clock period was performed as described with slight modifications.[12,106,117,118] For strain WT8–1, race tubes were filled with 15mL of Race Tube Media (1X Vogel's, 1.5% Agar, 0.05% Glucose, 0.17% L-Arginine, and Biotin 0.005 mg/mL), with cotton at the ends. For strains 328–4, 122, Ku-70a, and 1500–1, the same race tube media was prepared lacking glucose to facilitate conidial banding of non-banding strains. Tubes were inoculated at one end with conidia from slants grown on minimal media (see Fungal Genetics Stock Center website for recipe; 4–7 days of growth). Race tubes were grown in constant light (LL) at 25°C for 48 h before being moved to 25°C constant darkness (DD) and marked at their growth front every 24 h. WT8–1 tubes were analyzed for period using ChronOSX[119] and all other strains were analyzed by hand.

To obtain tissue for NS-LC-MS/MS analysis, conidia was grown on minimal media slants and then harvested by adding 50 mL of liquid culture media (LCM) and vortexing (see Fungal Genetics Stock Center website for recipe).[117] Harvested conidia were resuspended in 4L of LCM. 4L cultures of *N. crassa* were grown at 25°C in LL before being moved to constant dark conditions (DD) and sampled at different circadian times (Figure S2B). To obtain tissue for CRAFTY, conidia was grown on minimal media slants and harvested

in 4–7 days by adding 2 mL of LCM and vortexing. Harvested conidia were added to 20 mL of LCM in a Petri dish and left to grow at 25°C for one day in LL to form a mycelial mat. Plugs were cut from this mycelial mat and inoculated in 50 mL of LCM. *N. crassa* plugs were grown at 25°C in LL before being moved to constant dark conditions (DD) and sampled at different circadian times.

***Drosophila* strains and entrainment—**Flies expressing 3XFLAG-tagged dPER(WT),[111] or dPER(D755–809),[59] were entrained in a 12 h light/12 h dark (12:12 LD) cycle for 3 days at 25°C and collected on the fourth day at indicated time-points by flash freezing on dry ice.

METHOD DETAILS

Analysis of FRQ conform-ome using CRAFTY—CRAFTY assay and analysis was performed as described in Pelham et al. 2018.[30] Briefly, after the sample was grown for the allotted time, the culture was vacuum filtered and flash frozen, after which proteins were extracted using Protein Lysis Buffer with Halt™ Protease and Phosphatase Inhibitor Cocktail, EDTA Free diluted to a 1X concentration (Thermo Scientific™ 78441).[30] Protein concentration was measured by a Bradford Assay and standardized to 5 mg/mL at 4°C. Thermolysin (8.9 μM) was added to the samples and the samples were aliquoted to a thermocycler. Samples were heated to 25°C and at 15–30 s intervals the reaction was quenched using EDTA (20 mM) and SDS-PAGE loading buffer. Samples were analyzed using western blots, with 18.75μg of protein per lane in a 4–12% NuPAGE Bis-Tris gel. The primary antibody against the V5 tag on FRQ was sourced from Invitrogen (46–1157) and used at a 1:5000 dilution. The secondary antibody was Goat Anti-mouse IgG HRP conjugate sourced from Invitrogen (Invitrogen 31430) and used at a 1:25,000 dilution. For strain 1500–1, gels were imaged using a BioRad Gel Doc and image lab software (v. 6.0). An FRQ KO was loaded onto each gel to use as background removal during the quantification process. Each lane was normalized using amido black staining, followed by densitometry calculated from the initial time of digestion (time zero of protease addition). The digestion rate was quantified and converted into protease exposure half-life as in[29] using half-life kinetics from an exponential fit of the protease decay plot. WT8–1 CRAFTY gels were analyzed similarly, using Fiji rather than the BioRad Gel doc image lab.[110] The associated blots and stained membranes along with the data can be found in the Mendeley data link located in the key resources table.

Protein extraction and purification for mass spectrometric analyses of *Neurospora*—*Neurospora* tissue was harvested at the specified circadian times by vacuum filtration and proteins were extracted using Protein Lysis Buffer with Halt™ Protease and Phosphatase Inhibitor Cocktail, EDTA Free diluted to a 1X concentration (Thermo Scientific™ 78441).[30] Protein concentration was measured through Bradford Assay and standardized to 35 mg/mL 45 mL of total protein was transferred to washed/charged Ni-NTA agarose beads (Invitrogen™ R90110) and incubated for 1 h at 4°C with rotation before being washed. Proteins were eluted using Ni-NTA recommended elution buffer. All buffers were prepared as described in the manufacturer's instructions. The Ni-NTA eluted proteins were incubated with washed/pre-conjugated anti-FLAG magnetic

beads (Millipore™ M8823) overnight, washed, and eluted using Laemmle buffer. Beta-mercaptoethanol (BME) was added to an aliquot of protein elution for Western blot analysis.

Alkylation of cysteine residues—Proteins eluted from the anti-FLAG beads were reduced by adding 5mM of BME and incubated at 70°C for 20 min. Iodoacetamide was added to the sample to a final concentration of 13mM and incubated at room temperature in the dark for 1 h. The alkylation was quenched by adding an additional 5mM of BME at 25°C for 15 min.

Trichloroacetic acid precipitation and protein digestion—Alkylated protein products were mixed with cold 100% acetone and 100% trichloroacetic acid in a 1:8:1 ratio. This mixture was precipitated at −20°C for 1 h before centrifugation at 11,500 rpm for 15 min at 4°C. The supernatant was discarded, and the protein pellet washed with 1 mL of cold 100% acetone and centrifuged again at 11,500 rpm for 15 min at 4°C. The supernatant was again discarded, and the protein pellet was air dried. The protein pellet was resuspended in 190 μl of 50 mM ammonium bicarbonate and digested with 20 μl of 1 μg/μl trypsin gold (Promega V5280) at 37°C for 4 h.

Analysis of FRQ interactors by mass spectrometry—Samples were sent to the Mass-spec center at the University of Texas at Austin for analysis. Protein identification was performed via NS-LC-MS/MS using a Dionex Ultimate 3000 RSLCnano UPLC coupled to a Thermo Orbitrap Fusion. Prior to HPLC separation, the peptides were desalted using Millipore U-C18 ZipTip Pipette Tips following the manufacturer's protocol. A 2 cm long × 75 μm I.D. C18 trap column was followed by a 75 μm I.D. ×25 cm long analytical column packed with C18 3 μm material (Thermo Acclaim PepMap 100). Run-time was 1 h. The FT-MS resolution was set to 120,000, and 3 s cycle time MS/MS were acquired in ion trap mode. Raw data was processed using SEQUEST HT embedded in Proteome Discoverer. Scaffold (Proteome Software) was used for validation of peptide and protein identifications with filtering to achieve 99% protein confidence or a 1% FDR.

***Neurospora* interactome western blots—**FRQ, known FRQ interactors, and proteins of interest were verified through western blot analyses using the final purified protein elution from the FLAG pull down using a standard Western blot protocol.[29] Anti-V5 antibody (Invitrogen) was diluted 1:5,000. Anti-FLAG antibody was diluted 1:2,500 (F3165, Sigma). Immunodepleted anti-FRQ antibody was diluted 1:5000.[117] SuperSignal West Femto ECL (Pierce) was used for signal development. In order to verify that the purification process maintained FRQ's core interactions, we performed western blot analysis using anti-FRH[113] (diluted 1:10,000), anti-WC1[107] (diluted 1:250), and anti-WC2[108] (diluted 1:250). Secondary antibody was 1:5000 Goat anti-Rabbit (Invitrogen, 31460).

Fly protein extraction and affinity purification—Fly heads and bodies were separated using metal sieves and heads were used for protein extraction. Roughly 3 mL of heads were used per extraction. Fly heads were pulverized in liquid nitrogen and ground into fine powder using mortar and pestle. Powder was homogenized in lysis buffer as described above in (20 mM Hepes pH 7.4, 1 mM DTT, 0.1% Triton X-100, 0.5 mM phenylmethylsulfonyl fluoride (PMSF), supplemented with Complete EDTA-free Protease inhibitor cocktail

(Roche Life Sciences)) by using a 40 mL loose dounce homogenizer (Wheaton). The homogenate was filtered through 70um cell strainers (Corning Life Sciences, Tewsbury, MA) to remove fly debris before centrifugation to separate nuclei from cytoplasmic fraction. Lysed cells were centrifuged at 4°C, 2,000 rpm for 20 min. Supernatant was collected as cytoplasmic fraction and supplemented to get final Affinity Purification (AP) buffer composition of 20 mM Hepes pH 7.4, 1 mM DTT, 0.1% Triton X-100, 150 mM NaCl, 10% glycerol, 1 mM $MgCl_2$, 25 mM NaF, 0.5 mM EDTA, 0.5 mM PMSF, supplemented with Complete EDTA-free Protease inhibitor cocktail (Roche). Nuclear pellet was washed once with lysis buffer to eliminate any residual cytoplasmic extract. Proteins from nuclei were extracted with rotation for 1 h in nuclear extraction buffer (20 mM Hepes pH 7.4, 10% glycerol, 350 mM NaCl, 0.1% Triton X-100, 1 mM DTT, 1 mM $MgCl_2$, 0.5 mM EDTA, 25 mM NaF, 0.5 mM PMSF, supplemented with Complete EDTA-free Protease inhibitor cocktail (Roche)) at 4°C, along with the cytoplasmic fractions. 10 units of DNase I (Thermo Scientific, Waltham, MA) was added into the fractions during this one-hour incubation to minimize identification of non-specific protein interactions mediated by DNA-protein contacts. Post incubation, NaCl concentration for nuclear fraction was diluted down to 150 mM. Nuclear and cytoplasmic fractions were subsequently centrifuged at 27,000Xg for 15 min to remove cellular debris. Immunoprecipitation was performed at 4°C for 1 h and 30 min with 200 μL α-FLAG M2 beads (Sigma, St. Louis, MO) followed by four 10-min washes using AP buffer. Proteins were eluted twice with equal bead volume (200 μL) of AP buffer supplemented with 3XFLAG peptide (Sigma) at 200 μg/mL at room temperature for 15 min on a Nutator.

In-gel tryptic digestion and liquid chromatography-tandem mass spectrometry (LC-MS/MS) for *Drosophila* samples—To identify proteins bound to dPER, elutions were concentrated in a 14% Tris-Tricine gel and excised as a single gel slice. Each gel band was subjected to in-gel reduction, alkylation, tryptic digestion and peptide extraction as described in Qian et al. (2008). Peptides were solubilized in 0.1% trifluoroacetic acid and analyzed by Nano LC-MS/MS (Dionex Ultimate 3000 RLSC nano System interfaced with a Velos-LTQ-Orbitrap (Thermo Fisher, San Jose, CA). Samples were loaded onto a self-packed 100 μm × 2 cm trap (Magic C18AQ, 5μm 200Å, Michrom Bioresources, Inc.) and washed with Buffer A (0.2% formic acid) for 5 min with a flow rate of 10 μL/min. The trap was brought in-line with the analytical column (Magic C18AQ, 3 μm 200Å, 75 μm × 50 cm) and peptides fractionated at 250 nL/min using a segmented linear gradient: 4–25% B (0.2% formic acid in acetonitrile) in 60min, 25–55% B in 30 min. Mass spectrometry data was acquired using a data-dependent acquisition procedure with a cyclic series of a full scan acquired in Orbitrap with resolution of 60,000 followed by MS/MS (acquired in the linear ion trap) of the 20 most intense ions with a repeat count of two and a dynamic exclusion duration of 30 s.

QUANTIFICATION AND STATISTICAL ANALYSIS

***Neurospora* interactome data analysis—**To classify proteins as interactors (both in experimental and control conditions), protein thresholds in Scaffold were set at 99.9% and peptide thresholds were set at 95%, which are the minimum probability that a protein or peptide are identified in the spectra. Only proteins with ≥5% coverage or ≥4 unique peptides

were considered as “identified” in our dataset. All proteins identified in the Ku70 strain at all time points were pooled together and these proteins were removed from the list of proteins detected at any 1500–1 time point. The remaining proteins for each circadian time point in their respective grouping were compared and only proteins identified in at least two out of three of the triplicates were retained as valid FRQ interactors (Figure S2E). Expanded dataset can be found via Mendeley Data link in STAR key resources table.

To create the networking script, we used the experimental data derived from our MS/MS data to define the primary interactions and used the STRINGdb database to define the secondary interactions. These primary and secondary interactions were mapped to NCU identifiers from their STRINGdb ID using FungiDB and Uniprot. The GO analysis used the NCU identifiers as inputs and outputs to associate GO terms with each gene. The R package “iGraph” was used to graph the network using the Fruchterman-Reingold layout and each node was color coded by the GO terms associated with it in a pie chart style. The “vertex.size” variable in the plotting function was changed to match the number of total nodes to limit overlapping.

Transcriptomics and proteomics datasets were taken from the 48-h time series of *Neurospora crassa* from Hurley et al., 2018.[19] The imputed datasets were assessed for rhythmic gene expression or protein levels using the ECHO program.[109] Rhythms in gene expression were classified as significant if ECHO calculated the absolute value of the amplitude change coefficient to be less than 0.15, the Benjamini-Hochberg-adjusted p value less than 0.05, and the period between 20 and 28 h. Cell cycle genes and pathway information were taken from the KEGG (Kyoto Encyclopedia of Genes and Genomes) “Cell cycle - yeast – *Neurospora crassa*” pathway. The fitted dataset generated by ECHO from the triplicate time series was used for graphing and analysis. Peak expression times were the average of time points in CT corresponding to local maximums. Expression range was the difference between the average peak value and average trough value.

Analysis of dPER interactors by mass spectrometry—For protein identification from MS raw data, peak lists in MASCOT generic format (MGF) were generated using Proteome Discover 1.3 (ThermoFisher). Data were searched against Uniprot database for *Drosophila melanogaster* proteins using a local version of the Global Proteome Machine (GPM) XE Manager version 2.2.1 (Beavis Informatics Ltd., Winnipeg, Canada) with X! Tandem version 10–12-01–1 to assign spectral data (Beavis 2006). Precursor ion mass error tolerance was set to ±10 ppm and fragment mass error tolerance to ±0.4 Da. Cysteine carbamidomethylation was set as a complete modification, methionine oxidation and deamidation at asparagine and glutamine residues were set as variable modifications. All LC-MS data were analyzed together in a MudPit analysis and individual data extracted to ensure that peptides that could be assigned to more than one protein were assigned consistently for all samples. The resultant identifications were filtered by log GPM expectancy score (log(e)) of −5 for protein and −1 for peptide.

Spectral counts were utilized to establish a cutoff value, to discriminate between false and true interactors of dPER. If a protein had spectral counts ≤ 4, in 2 out of 3 replicates, the protein was removed from the final interactome list. Any protein found to interact with

dPER that had negative control spectral counts greater than or equal to 4, in 2 out of 3 replicates, was deemed a nonspecific interactor and was removed from all timepoints and fractionation. This approach to data processing filtered the spectral counts data to identify unique interactors for both wild type PER and PERΔ. Expanded dataset can be found via Mendeley Data link in STAR key resources table. After data processing, time point and sample type specific PPI lists were generated. To visualize the differences in PPIs between both time points and subcellular localization, Venn diagrams were created from the lists of interactors. The Venn diagrams were created in BioVenn[112] and jvenn.[47] This approach for comparative analysis was conducted on both WT PER and PERΔ datasets.

SLiM and computational analysis—The sequences of FRQ, dPER and hPER2 were run though the eukaryotic linear motif predictor (ELM).[57] The filter criteria were set for each organism, taxonomic cut offs were organism specific (FRQ as Fungi, dPER as *Drosophila melanogaster*, and hPER2 as *Homo sapiens*), and motif probability score of 100. Since the ELM database has a high rate of false positives, the SLiMs were verified and retained through their protein interactors by manually cross referencing with each interactome (FRQ with Dataset 1, dPER with Dataset 3 and hPER2 Oyama et al. 2019[21]). SLiMs were then plotted on a linear map of each protein (Figure 2). PTMs were plotted on each of the respective maps and curated from various sources (FRQ,[22] dPER,[72] and hPER2[114]). For the disorder plots FRQ, dPER and hPER2 sequences were run through the IUPred2A(L) tool which generated the disorder and ANCHOR prediction.[58]

Supplementary Material

Refer to Web version on PubMed Central for supplementary material.

ACKNOWLEDGMENTS

We thank Joshua Thomas for his assistance with creating the data processing script. We thank the Hurley lab members for their suggestions and support. We thank the Dunlap and Loros labs for strains and antibodies. *Neurospora* protein identification was provided by the UT Austin Center for Biomedical Research Support Biological Mass Spectrometry Facility (RRID: SCR_021728). This work was supported by NIH-National Institute of Biomedical Imaging and Bioengineering grant U01EB022546 (to J.M.H.); NIH-National Institute of General Medical Sciences grant R35GM128687 (to J.M.H.); NSF CAREER Award 2045674 (to J.M.H.); Rensselaer Polytechnic Startup funds (to J.M.H.); a gift from the Warren Alpert Foundation (to J.M.H.); and NIH-National Institute of Diabetes and Digestive and Kidney Diseases grant R01DK124068 (to J.C.C.). BioRender.com was used in the creation of the graphical abstract and Figure 6.

INCLUSION AND DIVERSITY

One or more of the authors of this paper self-identifies as a gender minority in their field of research. One or more of the authors of this paper received support from a program designed to increase minority representation in their field of research. We support inclusive, diverse, and equitable conduct of research.

REFERENCES

1. Dunlap JC (1999). Molecular bases for circadian clocks. Cell 96, 271–290. 10.1016/s0092-8674(00)80566-8. [PubMed: 9988221]

2. Decoursey PJ, Krulas JR, Mele G, and Holley DC (1997). Circadian performance of suprachiasmatic nuclei (SCN)-Lesioned antelope ground squirrels in a desert enclosure. Physiol. Behav 62, 1099–1108. 10.1016/s0031-9384(97)00263-1. [PubMed: 9333206]

3. Atamian HS, Creux NM, Brown EA, Garner AG, Blackman BK, and Harmer SL (2016). Circadian regulation of sunflower heliotropism, floral orientation, and pollinator visits. Science 353, 587–590. 10.1126/science.aaf9793. [PubMed: 27493185]

4. Partch CL, Green CB, and Takahashi JS (2014). Molecular architecture of the mammalian circadian clock. Trends Cell Biol. 24, 90–99. 10.1016/j.tcb.2013.07.002.Molecular. [PubMed: 23916625]

5. Hurley JM, Loros JJ, and Dunlap JC (2016). Circadian oscillators: around the transcription-translation feedback loop and on to output. Trends Biochem. Sci 41, 834–846. 10.1016/j.tibs.2016.07.009. [PubMed: 27498225]

6. Baker CL, Loros JJ, and Dunlap JC (2012). The circadian clock of Neurospora crassa. FEMS Microbiol. Rev 36, 95–110. 10.1111/j.1574-6976.2011.00288.x. [PubMed: 21707668]

7. Takahashi JS (2017). Transcriptional architecture of the mammalian circadian clock. Nat. Rev. Genet 18, 164–179. 10.1038/nrg.2016.150. [PubMed: 27990019]

8. Loros JJ (2020). Principles of the animal molecular clock learned from Neurospora. Eur. J. Neurosci 51, 19–33. 10.1111/ejn.14354. [PubMed: 30687965]

9. Crosthwaite SK, Dunlap JC, Loros JJ, Science S, Series N, May N, Crosthwaite SK, Dunlap JC, and Loros JJ (1997). Neurospora wc-1 and wc-2 : transcription , photoresponses , and the origins of circadian rhythmicity. Science 276, 763–769. [PubMed: 9115195]

10. Hurley JM, Dasgupta A, Emerson JM, Zhou X, Ringelberg CS, Knabe N, Lipzen AM, Lindquist EA, Daum CG, Barry KW, et al. (2014). Analysis of clock-regulated genes in Neurospora reveals widespread posttranscriptional control of metabolic potential. Proc. Natl. Acad. Sci. USA 111, 16995–17002. 10.1073/pnas.1418963111. [PubMed: 25362047]

11. Menet JS, Rodriguez J, Abruzzi KC, and Rosbash M (2012). Nascent-Seq reveals novel features of mouse circadian transcriptional regulation. Elife 2012, e00011–e00025. 10.7554/eLife.00011.

12. Loros JJ, Denome SA, and Dunlap JC (1989). Molecular cloning of genes under control of the circadian clock in Neurospora. Science 243, 385–388. [PubMed: 2563175]

13. Bell-Pedersen D, Cassone VM, Earnest DJ, Golden SS, Hardin PE, Thomas TL, and Zoran MJ (2005). Circadian Rhythms from Multiple Oscillators: Lessons from Diverse Organisms. Nat. Rev. Genet, 1–13. 10.1038/nrd1633.

14. Reddy AB, Karp NA, Maywood ES, Sage EA, Deery M, O'Neill JS, Wong GKY, Chesham J, Odell M, Lilley KS, et al. (2006). Circadian orchestration of the hepatic proteome. Curr. Biol 16, 1107–1115. 10.1016/j.cub.2006.04.026. [PubMed: 16753565]

15. Kojima S, Shingle DL, and Green CB (2011). Post-transcriptional control of circadian rhythms. J. Cell Sci 124, 311–320. 10.1242/jcs.065771. [PubMed: 21242310]

16. Robles MS, Cox J, and Mann M (2014). In-vivo quantitative proteomics reveals a key contribution of post-transcriptional mechanisms to the circadian regulation of liver metabolism. PLoS Genet. 10, e1004047. 10.1371/journal.pgen.1004047. [PubMed: 24391516]

17. Loros J, Dunlap JC, Larrondo LF, Hi MS, Elden WJB, Gooch VD Circadian Output, Input, and Intracellular Oscillators : Insights into the Circadian Systems of Single Cells. 2007. Cold Spring Harb. Symp. Quant. Biol p. LXXII.

18. Fuller KK, Hurley JM, Loros JJ, and Dunlap JC (2014). Photobiology and circadian clocks in *Neurospora*. Fungal Genomics, 121–148.

19. Hurley JM, Jankowski MS, De Los Santos H, Crowell AM, Fordyce SB, Zucker JD, Kumar N, Purvine SO, Robinson EW, Shukla A, et al. (2018). Circadian proteomic analysis uncovers mechanisms of post-transcriptional regulation in metabolic pathways. Cell Syst. 7, 613–626.e5. 10.1016/j.cels.2018.10.014. [PubMed: 30553726]

20. Collins EJ, Cervantes-Silva MP, Timmons GA, O'Siorain JR, Curtis AM, and Hurley JM (2021). Post-transcriptional circadian regulation in macrophages organizes temporally distinct immunometabolic states. Genome Res. 31, 171–185. 10.1101/gr.263814.120. [PubMed: 33436377]

21. Oyama Y, Bartman CM, Bonney S, Lee JS, Walker LA, Han J, Borchers CH, Buttrick PM, Aherne CM, Clendenen N, et al. (2019). Intense light-mediated circadian cardioprotection

via transcriptional reprogramming of the endothelium. Cell Rep. 28, 1471–1484.e11. 10.1016/j.celrep.2019.07.020. [PubMed: 31390562]

22. Baker CL, Kettenbach AN, Loros JJ, Gerber SA, and Dunlap JC (2009). Quantitative proteomics reveals a dynamic interactome and phase-specific phosphorylation in the Neurospora circadian clock. Mol. Cell 34, 354–363. 10.1016/j.molcel.2009.04.023. [PubMed: 19450533]
23. Mosier AE, and Hurley JM (2021). Circadian interactomics: how research into protein-protein interactions beyond the core clock has influenced the model of circadian timekeeping. J. Biol. Rhythms 36, 315–328. 10.1177/07487304211014622. [PubMed: 34056936]
24. Huang H, Alvarez S, Bindbeutel R, Shen Z, Naldrett MJ, Evans BS, Briggs SP, Hicks LM, Kay SA, and Nusinow DA (2016). Identification of evening complex associated proteins in arabidopsis by affinity purification and mass spectrometry. Mol. Cell. Proteomics 15, 201–217. 10.1074/mcp.m115.054064. [PubMed: 26545401]
25. Schmutz I, Ripperger JA, Baeriswyl-Aebischer S, and Albrecht U (2010). The mammalian clock component PERIOD2 coordinates circadian output by interaction with nuclear receptors. Genes Dev. 24, 345–357. 10.1101/gad.564110. [PubMed: 20159955]
26. Wallach T, Schellenberg K, Maier B, Kalathur RKR, Porras P, Wanker EE, Futschik ME, and Kramer A (2013). Dynamic circadian protein-protein interaction networks predict temporal organization of cellular functions. PLoS Genet. 9, e1003398. 10.1371/journal.pgen.1003398. [PubMed: 23555304]
27. Padmanabhan K, Robles MS, Westerling T, and Weitz CJ (2012). Feedback regulation of transcriptional termination by the mammalian circadian clock PERIOD complex. Science 337, 599–602. [PubMed: 22767893]
28. Mahesah G, Rivas G, Caster C, Ost E, Amunugama R, Jones R, Allen DL, and Hardin PE (2020). Proteomic Analysis of Drosophila CLOCK Complexes Identifies Rhythmic Interactions with SAGA and Tip60 Component NIPPED-A. Scientific Reports.
29. Hurley JM, Larrondo LF, Loros JJ, and Dunlap JC (2013). Conserved RNA helicase FRH acts nonenzymatically to support the intrinsically disordered neurospora clock protein FRQ. Mol. Cell 52, 832–843. 10.1016/j.molcel.2013.11.005. [PubMed: 24316221]
30. Pelham JF, Mosier AE, and Hurley JM (2018). Characterizing time-of-day conformational changes in the intrinsically disordered proteins of the circadian clock. Methods Enzymol. 611, 503–529. 10.1016/bs.mie.2018.08.024. [PubMed: 30471697]
31. Pelham JF, Dunlap JC, and Hurley JM (2020). Intrinsic disorder is an essential characteristic of components in the conserved circadian circuit.. Cell Commun. Signal 18, 181. [PubMed: 33176800]
32. Parico GCG, and Partch CL (2020). The tail of cryptochromes: an intrinsically disordered cog within the mammalian circadian clock. Cell Commun. Signal 18, 182. 10.1186/s12964-020-00665-z. [PubMed: 33198762]
33. Partch CL, Clarkson MW, Ozgür S, Lee AL, and Sancar A (2005). Role of structural plasticity in signal transduction by the cryptochrome blue-light photoreceptro. Biochemistry 44, 3795–3805. 10.1021/bi47545g. [PubMed: 15751956]
34. Uversky VN (2011). Intrinsically disordered proteins from A to Z. Int. J. Biochem. Cell Biol 43, 1090–1103. 10.1016/j.biocel.2011.04.001. [PubMed: 21501695]
35. Tompa P (2012). Intrinsically disordered proteins: a 10-year recap. Trends Biochem. Sci 37, 509–516. 10.1016/j.tibs.2012.08.004. [PubMed: 22989858]
36. Oldfield CJ, and Dunker AK (2014). Intrinsically disordered proteins and intrinsically disordered protein regions. Annu. Rev. Biochem 83, 553–584. 10.1146/annurev-biochem-072711-164947. [PubMed: 24606139]
37. Teilum K, Olsen JG, and Kragelund BB (2021). On the specificity of protein–protein interactions in the context of disorder. Biochem. J 478, 2035–2050. 10.1042/bcj20200828. [PubMed: 34101805]
38. Perovic V, Sumonja N, Marsh LA, Radovanovic S, Vukicevic M, Roberts SGE, and Veljkovic N (2018). IDPpi: protein-protein interaction analyses of human intrinsically disordered proteins. Sci. Rep 8, 10563. 10.1038/s41598-018-28815-x. [PubMed: 30002402]

39. Borgia A, Borgia MB, Bugge K, Kissling VM, Heidarsson PO, Fernandes CB, Sottini A, Soranno A, Buholzer KJ, Nettels D, et al. (2018). Extreme disorder in an ultrahigh-affinity protein complex. Nature 555, 61–66. 10.1038/nature25762. [PubMed: 29466338]
40. Bugge K, Brakti I, Fernandes CB, Dreier JE, Lundsgaard JE, Olsen JG, Skriver K, and Kragelund BB (2020). Interactions by disorder – a matter of context. Front. Mol. Biosci 7, 110. 10.3389/fmolb.2020.00110. [PubMed: 32613009]
41. Locasale JW (2008). Allovalency revisited: an analysis of multisite phosphorylation and substrate rebinding. J. Chem. Phys 128, 115106. 10.1063/1.2841124. [PubMed: 18361621]
42. Mittag T, Orlicky S, Choy W-Y, Tang X, Lin H, Sicheri F, Kay LE, Tyers M, and Forman-Kay JD (2008). Dynamic equilibrium engagement of a polyvalent ligand with a single-site receptor. Proc. Natl. Acad. Sci. USA 105, 17772–17777. 10.1073/pnas.0809222105. [PubMed: 19008353]
43. Wright PE, and Dyson HJ (2015). Intrinsically disordered proteins in cellular signalling and regulation. Nat. Rev. Mol. Cell Biol 16, 18–29. 10.1038/nrm3920. [PubMed: 25531225]
44. Dunker AK, Cortese MS, Romero P, Iakoucheva LM, and Uversky VN (2005). Flexible nets. The roles of intrinsic disorder in protein interaction networks. FEBS J. 272, 5129–5148. 10.1111/j.1742-4658.2005.04948.x. [PubMed: 16218947]
45. Kim PM, Sboner A, Xia Y, and Gerstein M (2008). The role of disorder in interaction networks: a structural analysis. Mol. Syst. Biol 4, 179. 10.1038/msb.2008.16. [PubMed: 18364713]
46. Querfurth C, Diernfellner ACR, Gin E, Malzahn E, Höfer T, and Brunner M (2011). Circadian conformational change of the neurospora clock protein FREQUENCY triggered by clustered hyperphosphorylation of a basic domain. Mol. Cell 43, 713–722. 10.1016/j.molcel.2011.06.033. [PubMed: 21884974]
47. Bardou P, Mariette J, Escudié F, Djemiel C, and Klopp C (2014). jvenn: an interactive Venn diagram viewer. BMC Bioinf. 15, 293. 10.1186/1471-2105-15-293.
48. Collett MA, Garceau N, Dunlap JC, and Loros JJ (2002). Light and clock expression of the neurospora clock gene frequency is differentially driven by but dependent on WHITE COLLAR-2. Genetics 160, 149–158. 10.1093/genetics/160.1.149. [PubMed: 11805052]
49. Wang B, Kettenbach AN, Zhou X, Loros JJ, and Dunlap JC (2019). The phospho-code determining circadian feedback loop closure and output in neurospora. Mol. Cell 74, 771–784.e3. 10.1016/j.molcel.2019.03.003. [PubMed: 30954403]
50. Edwards RJ, Paulsen K, and Aguilar Gomez CM (2020). In Pérez-BercoffÅ. Computational prediction of disordered protein motifs using SLiMSuite. Methods in Molecular Biology (Springer US), pp. 37–72. 10.1007/978-1-0716-0524-0_3.
51. Fuxreiter M, Tompa P, and Simon I (2007). Local structural disorder imparts plasticity on linear motifs. Bioinformatics 23, 950–956. 10.1093/bioinformatics/btm035. [PubMed: 17387114]
52. Davey NE, Van Roey K, Weatheritt RJ, Toedt G, Uyar B, Alten-berg B, Budd A, Diella F, Dinkel H, and Gibson TJ (2012). Attributes of short linear motifs. Mol. Biosyst 8, 268–281. 10.1039/c1mb05231d. [PubMed: 21909575]
53. Dinkel H, Van Roey K, Michael S, Davey NE, Weatheritt RJ, Born D, Speck T, Krüger D, Grebnev G, Kubań M, et al. (2014). The eukaryotic linear motif resource ELM: 10 years and counting. Nucleic Acids Res. 42, D259–D266. 10.1093/nar/gkt1047. [PubMed: 24214962]
54. Tang C-T, Li S, Long C, Cha J, Huang G, Li L, Chen S, and Liu Y (2009). Setting the pace of the Neurospora circadian clock by multiple independent FRQ phosphorylation events. Proc. Natl. Acad. Sci. USA 106, 10722–10727. 10.1073/pnas.0904898106. [PubMed: 19506251]
55. Liu Y, Loros J, and Dunlap JC (2000). Phosphorylation of the Neurospora clock protein FREQUENCY determines its degradation rate and strongly influences the period length of the circadian clock. Proc. Natl. Acad. Sci. USA 97, 234–239. 10.1073/pnas.97.1.234. [PubMed: 10618401]
56. Schafmeier T, Káldi K, Diernfellner A, Mohr C, and Brunner M (2006). Phosphorylation-dependent maturation of Neurospora circadian clock protein from a nuclear repressor toward a cytoplasmic activator. Genes Dev. 20, 297–306. 10.1101/gad.360906. [PubMed: 16421276]
57. Kumar M, Gouw M, Michael S, Sámano-Sánchez H, Pancsa R, Glavina J, Diakogianni A, Valverde JA, Bukirova D, Čalyševa J, et al. (2020). ELM—the eukaryotic linear motif resource in 2020. Nucleic Acids Res. 48, D296–D306. 10.1093/nar/gkz1030. [PubMed: 31680160]

58. Erdős G, and Dosztányi Z (2020). Analyzing protein disorder with IUPred2A. Curr. Protoc. Bioinformatics 70, e99. 10.1002/cpbi.99. [PubMed: 32237272]
59. Kim EY, Ko HW, Yu W, Hardin PE, and Edery I (2007). A DOUBLETIME kinase binding domain on the Drosophila PERIOD protein is essential for its hyperphosphorylation, transcriptional repression, and circadian clock function. Mol. Cell Biol 27, 5014–5028. 10.1128/mcb.02339-06. [PubMed: 17452449]
60. Cortese MS, Uversky VN, and Dunker AK (2008). Intrinsic disorder in scaffold proteins: getting more from less. Prog. Biophys. Mol. Biol 98, 85–106. 10.1016/j.pbiomolbio.2008.05.007. [PubMed: 18619997]
61. Good MC, Zalatan JG, and Lim WA (2011). Scaffold proteins: hubs for controlling the flow of cellular information. Science 332, 680–686. 10.1126/science.1198701. [PubMed: 21551057]
62. Morrison DK (2009). The 14-3-3 proteins: integrators of diverse signaling cues that impact cell fate and cancer development. Trends Cell Biol. 19, 16–23. 10.1016/j.tcb.2008.10.003. [PubMed: 19027299]
63. Clokie S, Falconer H, Mackie S, Dubois T, and Aitken A (2009). The interaction between casein kinase Iα and 14-3-3 is phosphorylation dependent. FEBS J. 276, 6971–6984. 10.1111/j.1742-4658.2009.07405.x. [PubMed: 19860830]
64. Yang W, Dicker DT, Chen J, and El-Deiry WS (2008). CARPs enhance p53 turnover by degrading 14-3-3σ and stabilizing MDM2. Cell Cycle 7, 670–682. 10.4161/cc.7.5.5701. [PubMed: 18382127]
65. Nielsen MD, Luo X, Biteau B, Syverson K, and Jasper H (2008). 14-3-3ϵ antagonizes FoxO to control growth, apoptosis and longevity inDro-sophila. Aging Cell 7, 688–699. 10.1111/j.1474-9726.2008.00420.x. [PubMed: 18665908]
66. Pacheco-Bernal I, Becerril-Pérez F, and Aguilar-Arnal L (2019). Circadian rhythms in the three-dimensional genome: implications of chromatin interactions for cyclic transcription. Clin. Epigenetics 11, 79. 10.1186/s13148-019-0677-2. [PubMed: 31092281]
67. Cha J, Zhou M, and Liu Y (2013). CATP is a critical component of the Neurospora circadian clock by regulating the nucleosome occupancy rhythm at the frequency locus. EMBO Rep. 14, 923–930. 10.1038/embor.2013.131. [PubMed: 23958634]
68. Raduwan H, Isola AL, and Belden WJ (2013). Methylation of histone H3 on lysine 4 by the lysine methyltransferase SET1 protein is needed for normal clock gene expression. J. Biol. Chem 288, 8380–8390. 10.1074/jbc.m112.359935. [PubMed: 23319591]
69. Ruesch CE, Ramakrishnan M, Park J, Li N, Chong HS, Zaman R, Joska TM, and Belden WJ (2014). The histone H3 lysine 9 methyltransferase DIM-5 modifies chromatin at frequency and represses light-activated gene expression. G3 5, 93–101. 10.1534/g3.114.015446. [PubMed: 25429045]
70. Lewis ZA, Adhvaryu KK, Honda S, Shiver AL, Knip M, Sack R, and Selker EU (2010). DNA methylation and normal chromosome behavior in Neurospora depend on five components of a histone methyltransferase complex, DCDC. PLoS Genet. 6, e1001196. 10.1371/journal.pgen.1001196. [PubMed: 21079689]
71. Bustos DM, and Iglesias AA (2006). Intrinsic disorder is a key characteristic in partners that bind 14-3-3 proteins. Proteins 63, 35–42. 10.1002/prot.20888. [PubMed: 16444738]
72. Garbe DS, Fang Y, Zheng X, Sowcik M, Anjum R, Gygi SP, and Sehgal A (2013). Cooperative interaction between phosphorylation sites on PERIOD maintains circadian period in Drosophila. PLoS Genet. 9, e1003749. 10.1371/journal.pgen.1003749. [PubMed: 24086144]
73. Bloom J, and Cross FR (2007). Multiple levels of cyclin specificity in cell-cycle control. Nat. Rev. Mol. Cell Biol 8, 149–160. 10.1038/nrm2105. [PubMed: 17245415]
74. Besson A, Dowdy SF, and Roberts JM (2008). CDK inhibitors: cell cycle regulators and beyond. Dev. Cell 14, 159–169. 10.1016/j.devcel.2008.01.013. [PubMed: 18267085]
75. Bendris N, Lemmers B, and Blanchard JM (2015). Cell cycle, cytoskeleton dynamics and beyond: the many functions of cyclins and CDK inhibitors. Cell Cycle 14, 1786–1798. 10.1080/15384101.2014.998085. [PubMed: 25789852]
76. Hong CI, Zámborszky J, Baek M, Labiscsak L, Ju K, Lee H, Larrondo LF, Goity A, Chong HS, Belden WJ, and Csikász-Nagy A (2014). Circadian rhythms synchronize mitosis in Neurospora

crassa. Proc. Natl. Acad. Sci. USA 111, 1397–1402. 10.1073/pnas.1319399111. [PubMed: 24474764]

77. Szklarczyk D, Gable AL, Lyon D, Junge A, Wyder S, Huerta-Cepas J, Simonovic M, Doncheva NT, Morris JH, Bork P, et al. (2019). STRING v11: protein-protein association networks with increased coverage, supporting functional discovery in genome-wide experimental datasets. Nucleic Acids Res. 47, D607–D613. 10.1093/nar/gky1131. [PubMed: 30476243]
78. The Gene Ontology Consortium; Douglass E, Dunn N, Good B, Harris NL, Lewis SE, Mungall CJ, Basu S, Chisholm RL, Dodson, et al. (2019). The gene ontology resource: 20 years and still GOing strong. Nucleic Acids Res. 47, D330–D338. 10.1093/nar/gky1055. [PubMed: 30395331]
79. Dreze M, Carvunis AR, Charloteaux B, Galli M, Pevzner SJ, Tasan M, Ahn YY, Balumuri P, Barabási AL, Bautista V, et al. (2011). Evidence for network evolution in an arabidopsis interactome map. Science 333, 601–607. [PubMed: 21798944]
80. De los Santos H, Bennett KP, Hurley JM (2020). MOSAIC: a joint modeling methodology for combined circadian and non-circadian analysis of multi-omics data. Bioinformatics 37, 767–774. 10.1101/2020.04.27.064147.
81. Mi H, Muruganujan A, Ebert D, Huang X, and Thomas PD (2019). PANTHER version 14: more genomes, a new PANTHER GO-slim and improvements in enrichment analysis tools. Nucleic Acids Res. 47, D419–D426. 10.1093/nar/gky1038. [PubMed: 30407594]
82. Caster SZ, Castillo K, Sachs MS, and Bell-Pedersen D (2016). Circadian clock regulation of mRNA translation through eukaryotic elongation factor eEF-2. Proc. Natl. Acad. Sci. USA 113, 9605–9610. 10.1073/pnas.1525268113. [PubMed: 27506798]
83. Simon I (2020). Macromolecular interactions of disordered proteins. Int. J. Mol. Sci 21, 504. 10.3390/ijms21020504. [PubMed: 31941113]
84. Mollica L, Bessa LM, Hanoulle X, Jensen MR, Blackledge M, and Schneider R (2016). Binding mechanisms of intrinsically disordered proteins: theory, simulation, and experiment. Front. Mol. Biosci 3, 52. 10.3389/fmolb.2016.00052. [PubMed: 27668217]
85. Arai M (2018). Unified understanding of folding and binding mechanisms of globular and intrinsically disordered proteins. Biophys. Rev 10, 163–181. 10.1007/s12551-017-0346-7. [PubMed: 29307002]
86. Wong DCS, Seinkmane E, Zeng A, Stangherlin A, Rzechorzek NM, Beale AD, Day J, Reed M, Peak-Chew SY, Styles CT, et al. (2022). CRYPTOCHROMES promote daily protein homeostasis. EMBO J. 41, e108883. [PubMed: 34842284]
87. Stangherlin A, Seinkmane E, and O'Neill JS (2021). Understanding circadian regulation of mammalian cell function, protein homeostasis, and metabolism. Curr. Opin. Syst. Biol 28, 100391. 10.1016/j.coisb.2021.100391.
88. Wang W, and Wang D (2019). Extreme fuzziness: direct interactions between two IDPs. Biomolecules 9, 81. 10.3390/biom9030081. [PubMed: 30813629]
89. Romero P, O'bradovic Z, Li X, Garner EC, Brown CJ, and Dunker AK (2001). Sequence complexity of disordered protein. Proteins 42, 38–48. [PubMed: 11093259]
90. Li X, Romero P, Rani M, and Dunker AK (1999). Predicting Protein Disorder for N-, C-, and Internal Regions. Genome Inform. Ser. Workshop Genome Inform
91. Obradovic Z, Peng K, Vucetic S, Radivojac P, Brown CJ, and Dunker AK (2003). Predicting intrinsic disorder from amino acid sequence. Proteins 53, 566–572. [PubMed: 14579347]
92. Mészáros B, Erdos G, and Dosztányi Z (2018). IUPred2A: context-dependent prediction of protein disorder as a function of redox state and protein binding. Nucleic Acids Res. 46, W329–W337. 10.1093/nar/gky384. [PubMed: 29860432]
93. Deiana A, Forcelloni S, Porrello A, and Giansanti A (2019). Intrinsically disordered proteins and structured proteins with intrinsically disordered regions have different functional roles in the cell. PLoS One 14, e0217889. 10.1371/journal.pone.0217889. [PubMed: 31425549]
94. Ghalwash MF, Dunker AK, and Obradović Z (2012). Uncertainty analysis in protein disorder prediction. Mol. Biosyst 8, 381–391. 10.1039/C1MB05373F. [PubMed: 22101336]
95. Peng K, Radivojac P, Vucetic S, Dunker AK, and Obradovic Z (2006). Length-dependant prediction of protein intrinsic disorder. BMC Bioinf 7, 208. 10.1186/1471-2105-7-208.

96. Gustafson CL, and Partch CL (2015). Emerging models for the molecular basis of mammalian circadian timing. Biochemistry 54, 134–149. 10.1021/bi500731f. [PubMed: 25303119]

97. Dubois T, Rommel C, Howell S, Steinhussen U, Soneji Y, Morrice N, Moelling K, and Aitken A (1997). 14-3-3 is phosphorylated by casein kinase I on residue 233. J. Biol. Chem 272, 28882–28888. 10.1074/jbc.272.46.28882. [PubMed: 9360956]

98. Pennington KL, Chan TY, Torres MP, and Andersen JL (2018). The dynamic and stress-adaptive signaling hub of 14-3-3: emerging mechanisms of regulation and context-dependent protein–protein interactions. Oncogene 37, 5587–5604. 10.1038/s41388-018-0348-3. [PubMed: 29915393]

99. Xiao Y, Yuan Y, Jimenez M, Soni N, and Yadlapalli S (2021). Clock proteins regulate spatiotemporal organization of clock genes to control circadian rhythms. Proc. Natl. Acad. Sci. USA 118, e2019756118. 10.1073/pnas.2019756118. [PubMed: 34234015]

100. Gabriel CH, Del Olmo M, Zehtabian A, Jäger M, Reischl S, Van Dijk H, Ulbricht C, Rakhymzhan A, Korte T, Koller B, et al. (2021). Live-cell imaging of circadian clock protein dynamics in CRISPR-generated knock-in cells. Nat. Commun 12, 3796. 10.1038/s41467-021-24086-9. [PubMed: 34145278]

101. Beesley S, Kim DW, D'Alessandro M, Jin Y, Lee K, Joo H, Young Y, Tomko RJ, Faulkner J, Gamsby J, et al. (2020). Wake-sleep cycles are severely disrupted by diseases affecting cytoplasmic homeostasis. Proc. Natl. Acad. Sci. USA 117, 28402–28411. 10.1073/pnas.2003524117. [PubMed: 33106420]

102. Huang H, and Nusinow DA (2016). Into the evening: complex interactions in the arabidopsis circadian clock. Trends Genet. 32, 674–686. 10.1016/j.tig.2016.08.002. [PubMed: 27594171]

103. Aryal RP, Kwak PB, Tamayo AG, Gebert M, Chiu PL, Walz T, and Weitz CJ (2017). Macromolecular assemblies of the mammalian circadian clock. Mol. Cell 67, 770–782.e6. 10.1016/j.mol-cel.2017.07.017. [PubMed: 28886335]

104. Guo J, Cheng P, Yuan H, and Liu Y (2009). The exosome regulates circadian gene expression in a posttranscriptional negative feedback loop. Cell 138, 1236–1246. 10.1016/j.cell.2009.06.043. [PubMed: 19747717]

105. Aryal UK, Ding Z, Hedrick V, Sobreira TJP, Kihara D, and Sherman LA (2018). Analysis of protein complexes in the unicellular cyano-bacterium cyanothece ATCC 51142. J. Proteome Res 17, 3628–3643. 10.1021/acs.jproteome.8b00170. [PubMed: 30216071]

106. Gooch VD, Mehra A, Larrondo LF, Fox J, Touroutoutoudis M, Loros JJ, and Dunlap JC (2008). Fully codon-optimized luciferase uncovers novel temperature characteristics of the Neurospora clock. Eukaryot. Cell 7, 28–37. 10.1128/EC.00257-07. [PubMed: 17766461]

107. Lee K, Loros JJ, and Dunlap JC (2000). Interconnected feedback loops in the neurospora circadian system. Science 289, 107–110. 10.1126/science.289.5476.107. [PubMed: 10884222]

108. Denault DL, Loros JJ, and Dunlap JC (2001). WC-2 mediates WC-1-FRQ interaction within the PAS protein-linked circadian feedback loop of Neurospora. EMBO J. 20, 109–117. 10.1093/emboj/20.1.109. [PubMed: 11226161]

109. De los Santos H, Collins EJ, Mann C, Sagan AW, Jankowski MS, Bennett KP, and Hurley JM (2020). ECHO: an application for detection and analysis of oscillators identifies metabolic regulation on genome-wide circadian output. Bioinformatics 36, 773–781. 10.1101/690941. [PubMed: 31384918]

110. Schindelin J, Arganda-Carreras I, Frise E, Kaynig V, Longair M, Pietzsch T, Preibisch S, Rueden C, Saalfeld S, Schmid B, et al. (2012). Fiji: an open-source platform for biological-image analysis. Nat. Methods 9, 676–682. 10.1038/nmeth.2019. [PubMed: 22743772]

111. Li YH, Liu X, Vanselow JT, Zheng H, Schlosser A, and Chiu JC (2019). O-GlcNAcylation of PERIOD regulates its interaction with CLOCK and timing of circadian transcriptional repression. PLoS Genet. 15, e1007953. 10.1371/journal.pgen.1007953. [PubMed: 30703153]

112. Hulsen T, De Vlieg J, and Alkema W (2008). BioVenn – a web application for the comparison and visualization of biological lists using area-proportional Venn diagrams. BMC Genom. 9, 488. 10.1186/1471-2164-9-488.

113. Shi M, Collett M, Loros JJ, and Dunlap JC (2010). FRQ-interacting RNA helicase mediates negative and positive feedback in the neurospora circadian clock. Genetics 184, 351–361. 10.1534/genetics.109.111393. [PubMed: 19948888]

114. Hornbeck PV, Zhang B, Murray B, Kornhauser JM, Latham V, and Skrzypek E (2015). PhosphoSitePlus, 2014: mutations, PTMs and recalibrations. Nucleic Acids Res. 43, D512–D520. 10.1093/nar/gku1267. [PubMed: 25514926]

115. Colot HV, Park G, Turner GE, Ringelberg C, Crew CM, Litvin-kova L, Weiss RL, Borkovich KA, and Dunlap JC (2006). A high-throughput gene knockout procedure for Neurospora reveals functions for multiple transcription factors. Proc. Natl. Acad. Sci. USA 103, 10352–10357. 10.1073/pnas.0601456103. [PubMed: 16801547]

116. Bardiya N, and Shiu PKT (2007). Cyclosporin A-resistance based gene placement system for Neurospora crassa. Fungal Genet. Biol 44, 307–314. 10.1016/j.fgb.2006.12.011. [PubMed: 17320431]

117. Garceau NY, Liu Y, Loros JJ, and Dunlap JC (1997). Alternative initiation of translation and time-specific phosphorylation yield multiple forms of the essential clock protein FREQUENCY. Cell 89, 469–476. 10.1016/s0092-8674. [PubMed: 9150146]

118. Ruoff P, Loros JJ, and Dunlap JC (2005). The relationship between FRQ-protein stability and temperature compensation in the Neurospora circadian clock. Proc. Natl. Acad. Sci. USA 102, 17681–17686. 10.1073/pnas.0505137102. [PubMed: 16314576]

119. Roenneberg T, and Taylor W (2000). In Automated recordings of bioluminescence with special reference to the analysis of circadian rhythms. Bioluminescence and Chemiluminescence Part (Elsevier), pp. 104–119. 10.1016/s0076-6879(00)05481-1.

Highlights

- Negative-arm circadian clock proteins display time-specific conformations
- Eukaryotes have spatiotemporally dynamic core clock-centered protein complexes
- SLiMs and protein disorder are conserved drivers of circadian regulation
- The negative arm imparts circadian post-transcriptional regulation of physiology

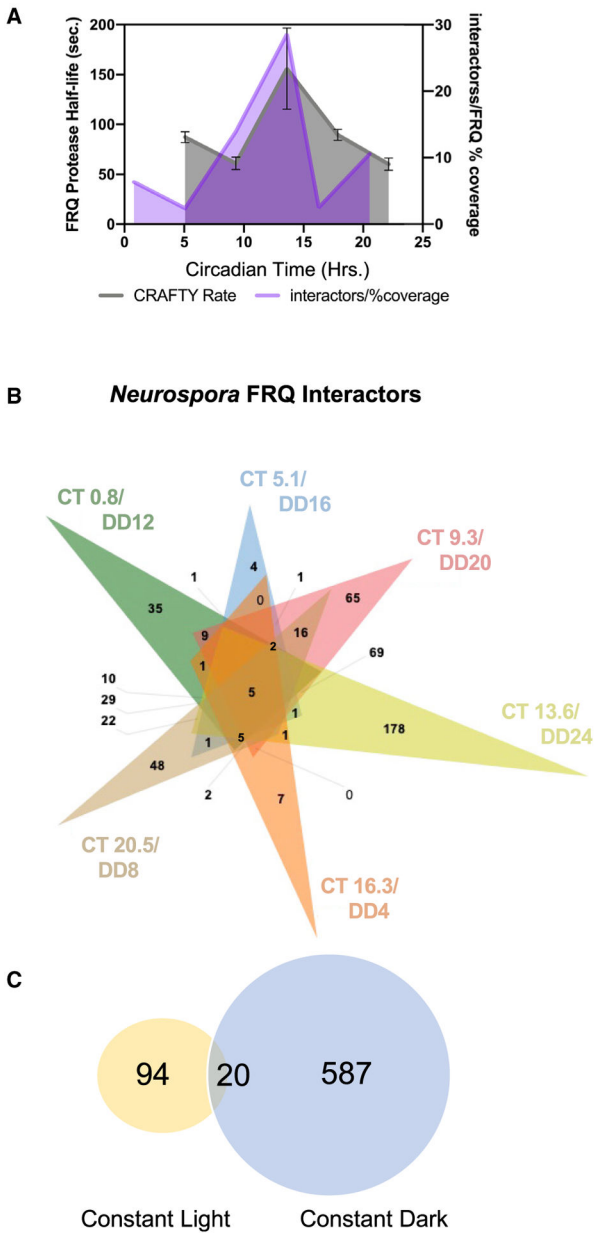

Figure 1. FRQ protease resistance and interactomes vary over the circadian day

(A) The protease resistance of FRQ, represented as protein half-life (gray), was plotted on the same graph as the number of FRQ interactors normalized to the precent coverage of FRQ in each pull down (see methods) (purple) at the same circadian time (CT) and shaded for ease of comparison. Error bars represent standard error of the means (SEM, n = 3).

(B) Complex Venn diagram that is not scaled displaying the overlap between proteins identified in complex with FRQ at different time points over the circadian day (CT0.8/DD12 in green, CT5.1/DD16 in cyan, CT9.3/DD20 in pink, CT13.6/DD24 in yellow, CT16.3/DD4 in orange, and CT20.5/DD8 in tan).[47]

(C) Venn diagram displaying the overlap between proteins identified in complex with FRQ in LL (yellow) or DD (blue).

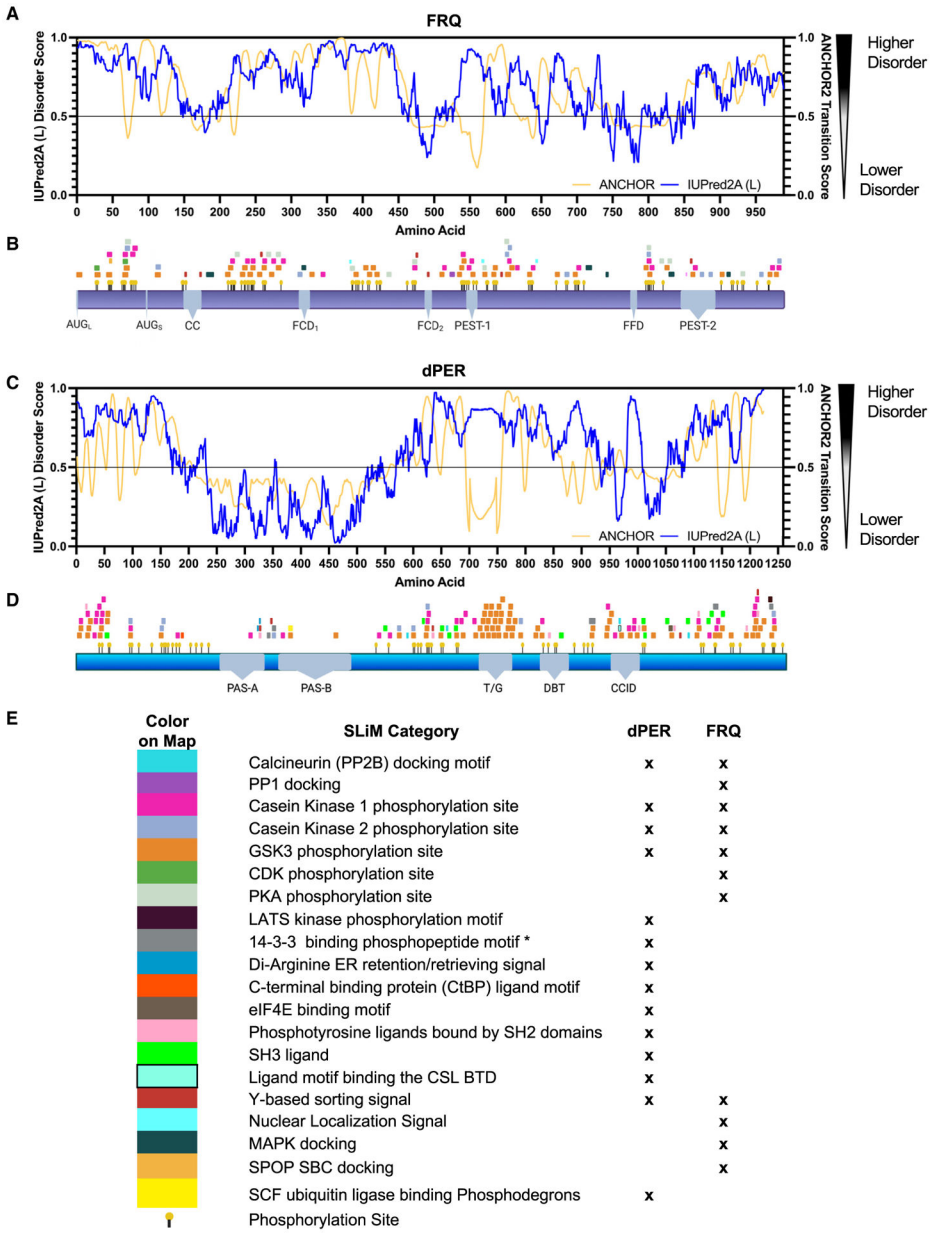

Figure 2. Sequential analysis of negative-arm elements demonstrates interactome-confirmed SLiM regulation sites in disordered regions

(A and C) A linear representation of the disorder propensity and disorder to order transition upon binding for FRQ and dPER, respectively, calculated using IUPred2A(L) and ANCHOR2.[58]

(B and D) A linear map of ELM computationally predicted FRQ and dPER SLiMs, respectively, that had interactors identified in the LC-MS/MS analysis.[57] SLiMs and PTMs were mapped to their location on FRQ[22] and dPER. Known FRQ domains are highlighted in gray and phosphosites as yellow pins. Regions of interest are denoted as follows: long and short start codons, AUG_L and AUG_S; CC, coiled-coil domain for FRQ dimerization; FCD_1 and FCD_2, FRQ and CK1 interaction region; FFD, FRQ and FRH interaction region.[30] Known dPER domains are highlighted in gray (PAS-A and PAS-B, PER-ARNT-

SIM domains; T/G, threonine glycine-rich region; DBT, DOUBLETIME interacting region; CCID, dCLK and CYC inhibition domain) and phophosites as yellow pins.
(E) SLiM legend, each SLiM category is represented by its corresponding color. An X in the FRQ or dPER column indicates the presence of the SLiM on each respective map.

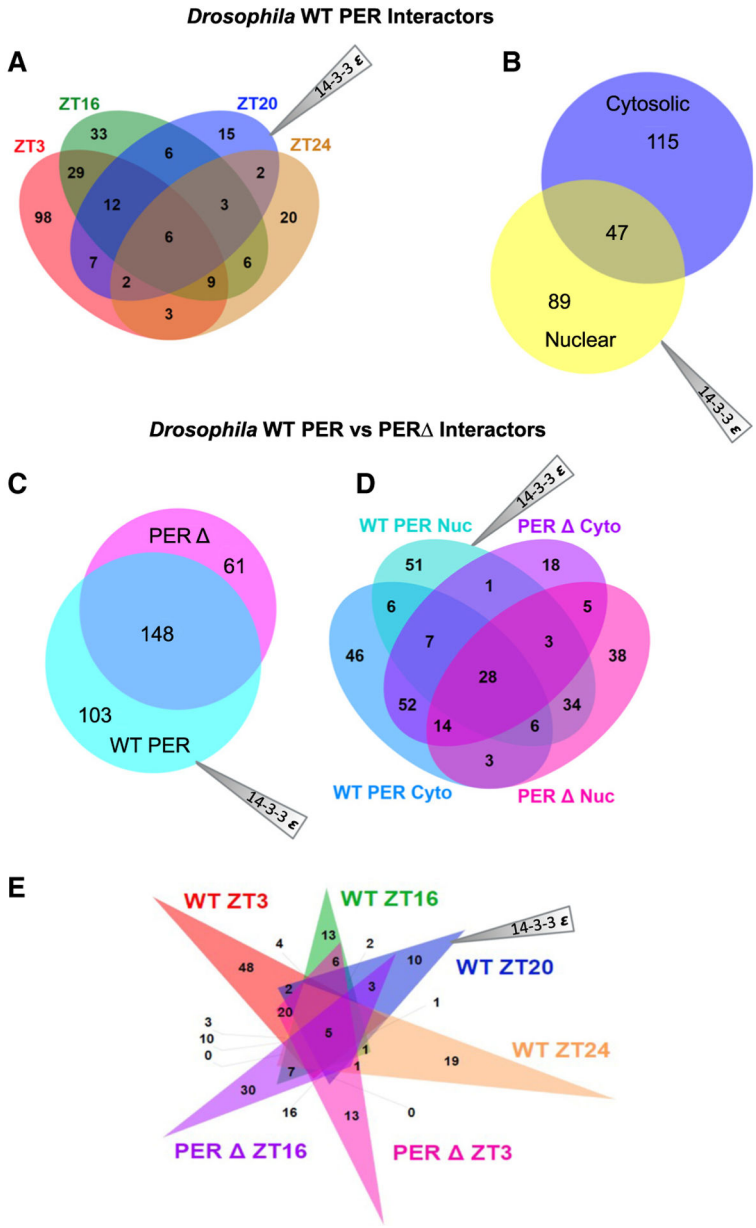

Figure 3. Macromolecular complexes centered around dPER are spatiotemporally specific

(A) Comparison of proteins identified in complex with dPER in wild-type (WT) samples grouped by time point (ZT3: salmon, ZT16: green, ZT20: blue, and ZT24: tan).

(B) Comparison of proteins identified in complex with dPER in WT samples grouped by subcellular localization (cytosolic: blue and nuclear: yellow).

(C) Comparison of dPER interactors in all WT and PER Δ samples (WT: cyan and PER Δ: pink).

(D) Comparison of WT and PER Δ grouped by subcellular localization (WT/cytosolic: blue, WT/nuclear: cyan, PER Δ/cytosolic: purple, PER Δ/nuclear: pink).

(E) Comparison of WT and PER Δ grouped by time point (WT/ZT3: salmon, WT/ZT16: green, WT/ZT20: blue, WT/ZT24: tan, PER Δ/ZT3: pink, PER Δ/ZT16: purple).

Gray shaded triangle in all panels indicates identified 14-3-3 protein.

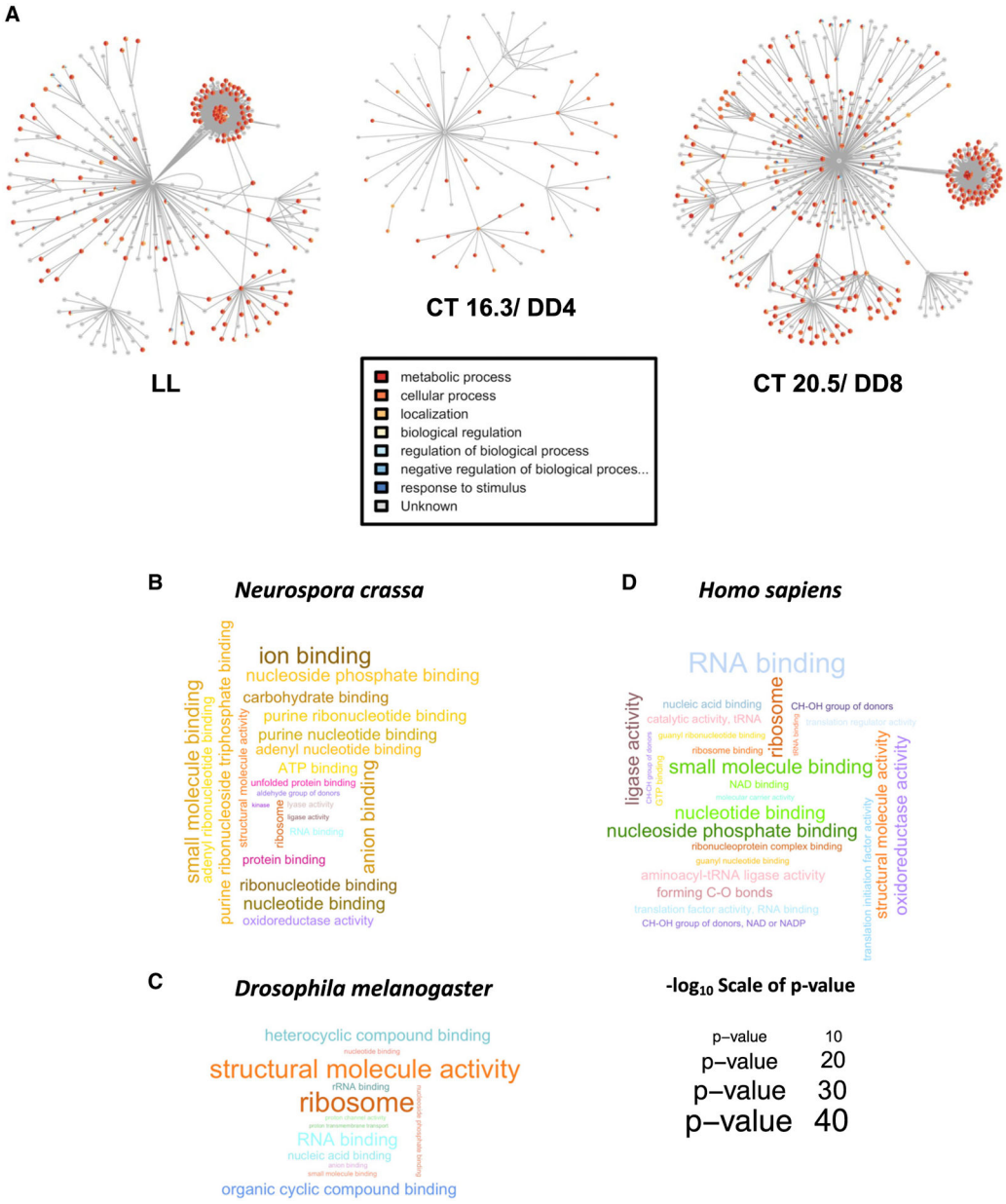

Figure 4. Negative-arm macromolecular complexes oscillate in composition and physiological function over the circadian day

(A) Protein interaction maps exhibiting the FRQ interactome at different time points (shown as examples are LL, CT16.3/DD4, and CT20.5/DD8). FRQ is in the center with radial lines connecting to proteins identified by LC-MS/MS. Predicted secondary interactors are connected to their respective primary interactor. Nodes are color coded for the secondary gene ontology (GO) term shown.

(B–D) Word clouds related to the enriched GOs of the interactions, created using terms with a higher than 2-fold enrichment and p value >0.05, with the magnitude of each term represented by the −log10 of its p value for FRQ (B), dPER (C), and hPER (D) and colors indicating each GO family with a color key in Table S2. The scaled p value legend indicates the level of enrichment.

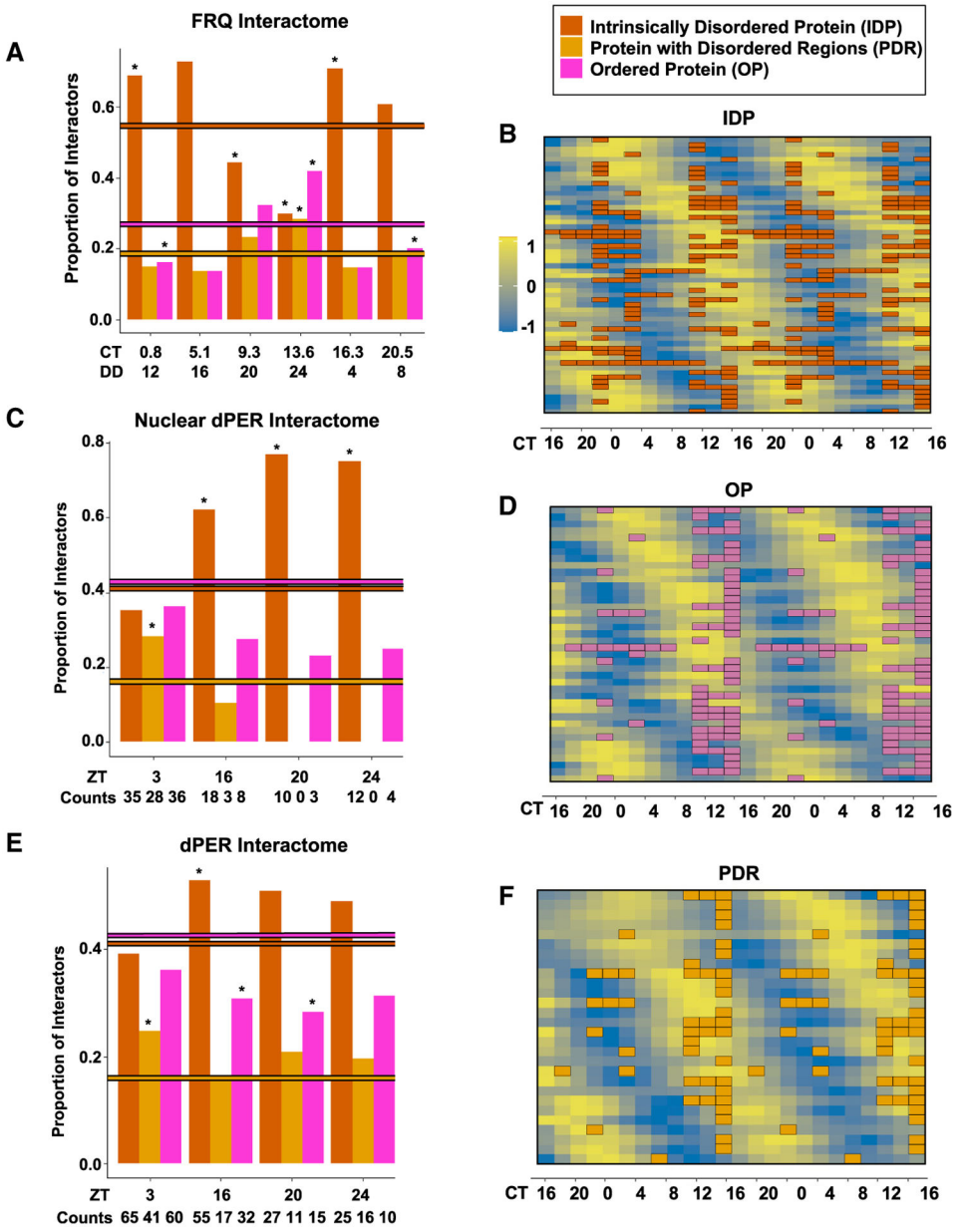

Figure 5. IDP/negative-arm protein interactions oscillate over the circadian day

(A) Bar plot showing the proportion and enrichment of IDPs, PDRs, and OPs in FRQ macromolecular complexes at a given time point compared with the proportion of IDPs, PDRs, and OPs in the full *N. crassa* proteome (horizontal lines) (p values assessed by Fisher's exact test *$p < 0.05$).

(B, D, and F) Heatmaps showing global protein levels for oscillating, FRQ-interacting proteins, IDPs (B), PDRs (F), and OPs (D) as reported in Hurley et al.[19] These global protein levels are overlaid with the times of day that the corresponding protein interacted with FRQ for each IDP (orange), PDR (yellow), or OP (purple).[19]

(C and E) Bar plot showing the proportion and enrichment of IDPs, PDRs, and OPs in dPER macromolecular complexes at a given time point compared with the proportion of IDPs,

PDRs, and OPs in the full *D. melanogaster* proteome (horizontal lines) (p values assessed by Fisher's exact test $p < 0.05$) in the total *D. melanogaster* interactome (C) and the nuclear *D. melanogaster* interactome (E).

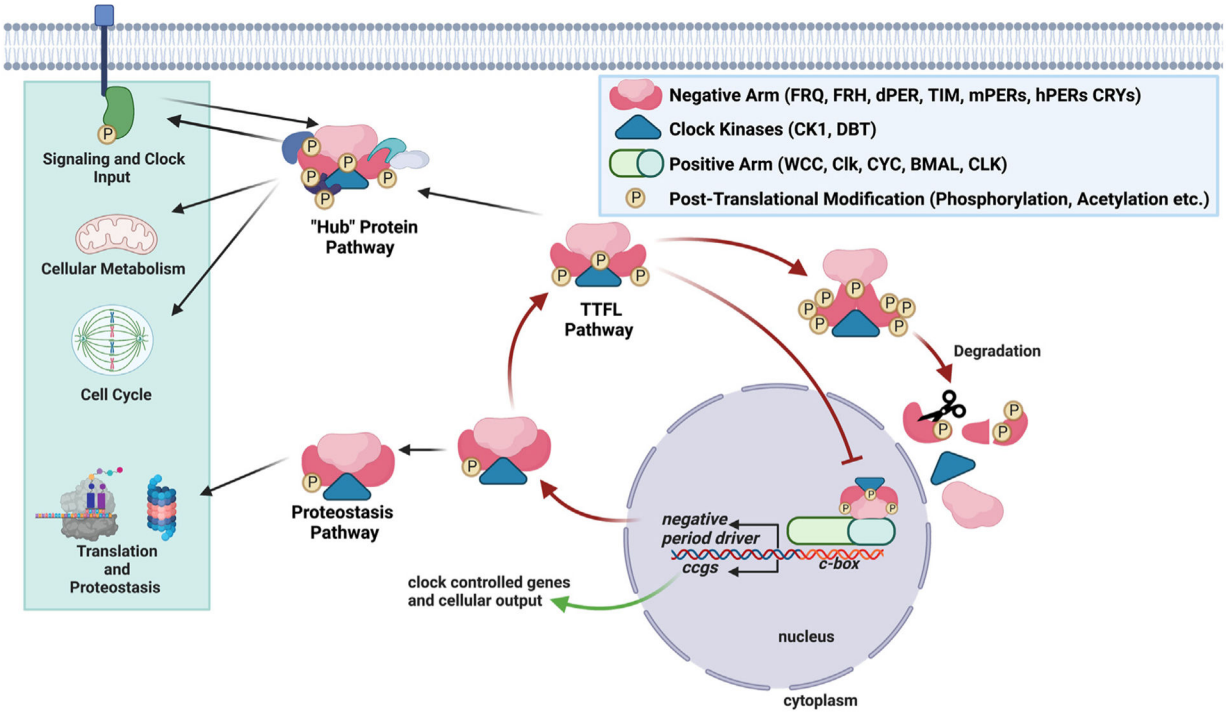

Figure 6. Clock negative-arm proteins may act as a source of post-transcriptional clock regulation by acting as temporal "Hub" proteins and/or "proteostasis" regulators

Schematic representation of the classical circadian TTFL and the mechanisms by which we propose methods of negative-arm post-transcriptional regulation occur. Proteins that bind negative-arm macromolecular complexes can be temporally stabilized or phosphorylated, leading to downstream circadian post-transcriptional regulation in a variety of cellular pathways.

KEY RESOURCES TABLE

REAGENT or RESOURCE	SOURCE	IDENTIFIER
Antibodies		
V5 Tag Monoclonal Antibody	Invitrogen	Cat# 46–1157
Goat anti-Mouse IgG (H+L) Secondary Antibody HRP	Invitrogen	Cat# 31430
Monoclonal ANTI-FLAG M2 antibody	Sigma	Cat# F3165; RRID:AB_259529
Anti-FRQ (Rabbit)	Jay Dunlap[106]	N/A
Anti-FRH	Jay Dunlap[107]	N/A
Anti-WC-1	Jay Dunlap[108]	N/A
Anti-WC-2	Jay Dunlap[109]	N/A
Goat anti-Rabbit IgG (H+L) Secondary Antibody HRP	Invitrogen	Cat# 31460
Chemicals, peptides, and recombinant proteins		
Halt Protease and Phosphatase Inhibitor Cocktail EDTA Free	ThermoFisher Scientific	Cat# 78441
NuPAGE Gel 4–12% Bis-Tris	Invitrogen	Cat# WG1402BOX
Ni-NTA Agarose	Invitrogen	Cat# R90110
Anti-FLAG M2 Affinity Gel	Millipore Sigma	Cat# A2220
Trypsin Gold	Promega	Cat# V5280
SuperSignal West FEMTO	ThermoFisher Scientific	Cat# 34094
cOmplete, EDTA-free protease Inhibitor Cocktail	Roche	Cat# 04693132001
DNase I	ThermoFisher Scientific	Cat# EN0521
3XFLAG Peptide	Sigma	Cat# F4799
Deposited data		
Mendelay data links	This Paper	https://data.mendeley.com/v1/datasets/cshd5drzp5/draft?a=99cee2fb-f059-40f3-b825-ce9f3f0badff
Experimental models: Organisms/strains		
N. crassa: WT8–1: csr-1::frq ^{v5his103flag} , ras-1 ^{bd}	This Paper	N/A
N. crassa: 328–4: ras-1 ^{bd} , mat A	Fungal Genetics Stock Center	N/A
N. crassa:122: ras-1 ^{bd} , ΔFRQ::hph+, mat a	Jay Dunlap	N/A
N. crassa: frq ^{V5H103FLAG} ::hph+	This paper	N/A
N. crassa: Ku70::bar, NCU04424.1::hph, mat a	Fungal Genetics Stock Center	N/A
D. melanogaster: dPER WT: wper0; p{3XFLAG-per(13.2WT)-HA10HIS}	Joanna Chiu[110]	N/A
D. melanogaster: dPERΔ wper0; p{3XFLAG-per(Δ)-HA10HIS}	Joanna Chiu[59]	N/A
Oligonucleotides		
See Table S2		N/A
Software and algorithms		
ChronOSX 2.1	Roennenberg et al. 2000[111]	N/A
ECHO	De los Santos et al. 2020[112]	https://github.com/delosh653/ECHO
Fiji	Schindelin et al. 2012[113]	https://imagej.nih.gov/ij/download.html
VSL2b	Peng et al. 2006[96]	http://www.pondr.com/pondr-tut2.html

REAGENT or RESOURCE	SOURCE	IDENTIFIER
VLXT	Romero et al. 2001[89]	http://www.pondr.com/pondr-tut2.html
PV2	Ghalwash et al. 2012[95]	https://d2p2.pro/about/predictors
BioVenn	Hulsen at al. 2008[114]	https://www.biovenn.nl
Jvenn	Bardou et al. 2014[115]	http://jvenn.toulouse.inra.fr/app/index.html
Image Lab v. 6.0	BioRad	N/A
IUPred2AL	Erdős et al. 2020[93]	https://iupred2a.elte.hu
Circadian PPIN Scripts	This Paper	https://doi.org/10.5281/zenodo.7741908